Original article

Collisional bending of the western Paleo-Kuril Arc deduced from paleomagnetic analysis and U-Pb age determination

Takahiro Katagiri [a, *, 1], Hajime Naruse [a], Naoto Ishikawa [b] and Takafumi Hirata [a, 2]

[a] *Graduate School of Science, Kyoto University, Kyoto 606-8502, Japan*

[b] *Graduate School of Human and Environmental Studies, Kyoto University, Kyoto 606-8501, Japan*

[1] *Now at INPEX Corp.*

[2] *Now at The University of Tokyo*

[*] *Corresponding author: T. Katagiri*

E-mail: katagiri.takahiro@gmail.com

Abstract

The Paleo-Kuril Arc in the eastern Hokkaido region of Japan, the westernmost part of the Kuril Arc in the northwestern Pacific region, shows a tectonic bent structure. This has been interpreted, using paleomagnetic data, to be the result of block rotations in the Paleo-Kuril Arc. To understand the timing and origin of this tectonic bent structure in the Paleo-Kuril arc-trench system, paleomagnetic surveys and U-Pb radiometric dating were conducted in the Paleogene Urahoro Group, which is distributed in the Shiranuka-hill region, eastern Hokkaido. The U-Pb radiometric dating indicated that the Urahoro Group was deposited at approximately 39 Ma. Paleomagnetic analysis of the Urahoro Group suggested that the Shiranuka-hill region experienced a 28° clockwise rotation with respect to East Asia. The degree of clockwise rotation implied from the Urahoro Group is smaller than that of the underlying Lower Eocene Nemuro Group (62°) but larger than that of the overlying Onbetsu Group (-9°). It is thus suggested that the Shiranuka-hill region experienced a clockwise rotation of approximately 34° between the deposition of the Nemuro and Urahoro groups (50–39 Ma), and a 38° clockwise rotation between the deposition of the Urahoro and Onbetsu groups (39–34 Ma). The origin of the curved tectonic belt of the Paleo-Kuril Arc was previously explained by the opening of the Kuril Basin after 34 Ma. The age constraint for the rotational motion of the Shiranuka-hill region in this study contradicts this hypothesis. Consequently, it is suggested that the process of arc-arc collision induced the bent structure of the western Paleo-Kuril Arc.

Keywords

Arc-Arc collision, Paleo-Kuril Arc, Paleomagnetism, U-Pb radiometric dating

1. Introduction

Bent structures of tectonic belts are globally common in various tectonic settings. They are recognized from their contorted spatial distribution and rotation of terranes, as detected by paleomagnetic declination (Duermeijer, Nyst, Meijer, Langereis & Spakman, 2000; Otofuji, Enami, Yokoyama, Kamiya, Kuma, Saito & Matsuda, 1999; Takahashi & Saito, 1997). These bent structures of tectonic belts can be formed as a result of large-scale tectonic events, including convergence of continental blocks or opening of back-arc basins, which generally accompany orogeny (e.g. Kano, 2002; Klootwijk, Conaghan, & Powell, 1985; McCabe, 1984). For example, the opening of the Japan Sea (the back arc basin of Japanese Island arcs) and collision of the Izu-Bonin Arc caused a large-scale bent structure of the tectonic belts of the Japanese Island arc system (e.g. Otofuji, 1996; Takahashi & Saito, 1997). Similarly, the collision of Gondwana with Laurasia produced the curved mountain belts of the Cantabria-Asturias arc (Weil, Voo, & Pluijm, 2001).

Tectonic belts in the western part of the Paleo-Kuril Arc, the eastern part of the Hokkaido Island of northernmost Japan, exhibit a large-scale bent structure (Fujiwara, Kanamatsu, & Nanayama, 1995; Kimura, 1990, 1993). Structural trends of the tectonic belts in this region significantly vary at the Kushiro marsh (Figure 1). Pre-Neogene terranes distributed in the Konsen-coastal region extend from east to west, while they extend from north to south in the Shiranuka-hill region (Figure 1). In addition, clockwise-deflected paleomagnetic declinations are reported for those in the western region. Thus, tectonic belts in the Paleo-Kuril Arc originally extended in an east-west direction parallel to the Arc-Trench system, and the tectonic belts in this area were bent after their deposition (Fujiwara et al., 1995; Fujiwara & Kanamatsu, 1994; Kanamatsu, Nanayama, Iwata, & Fujiwara, 1992; Kimura, 1990, 1993; Nanayama, Kanamatsu, & Fujiwara, 1993).

The formation of the bent structure in the Paleo-Kuril Arc occurred during the Eocene (Fujiwara et al., 1995; Figure 2). Paleomagnetic surveys in the Shiranuka-hill region in the western part of the bent structure (Figure 1) provide the age constraints for this tectonic event. The Upper Cretaceous to Middle Eocene Nemuro Group shows clockwise deflections in paleomagnetic declination from the geographic north, while the uppermost Eocene to early Oligocene Onbetsu Group shows no deflection (Fujiwara et al., 1995; Hamano, Tsunakaawa, Saito, & Kikawa, 1986; Kaiho, 1983, 1984). Although the paleomagnetic direction from the Urahoro Group, which is on the Nemuro Group and overridden by the Onbetsu Group, was also measured by Fujiwara et al. (1995), it is not reliable because of an inaccurate process in their demagnetization experiments (see later discussion). Therefore, the existing paleomagnetic data suggest that the bent structure was formed between the depositions of the Nemuro and Onbetsu groups (Middle Eocene–Early Oligocene).

The origin of the bent structure is ambiguous due to this weak constraint of the age of formation. Between the deposition of the Nemuro and Onbetsu groups, there were two significant tectonic events (Figure 2). One was a collision between the Paleo-Kuril Arc and Paleo-Northeastern Japan Arc and the other was a spreading of the Kuril Basin. The former event was estimated to have started before the deposition of the Urahoro Group (Iijima, 1996; Kiminami, 2010; Kimura & Kusunoki, 1997), although the latter was estimated to have occurred after the deposition of the Urahoro Group (Fukusawa & Ishihara, 1992; Iijima & Tada, 1990; Kimura & Tamaki, 1985; Maeda, 1990).

In order to determine the age of formation of the bent structure precisely, we conducted paleomagnetic surveys and U-Pb radiometric dating of the Urahoro Group. Our data implies that the bent structure of the western end of the Paleo-Kuril Arc was formed both before and after the deposition of the Urahoro group. Because the block rotation occurred before the deposition of the Urahoro Group, it cannot have been due to the spreading of the Kuril Basin and therefore we conclude that the bent structure was mainly caused by the collision of the Paleo-Kuril Arc and the Paleo-Northeastern Japan Arc.

2. Geological setting

Hokkaido Island is located in the northern part of the Japanese Archipelago. Tectonic belts in Hokkaido Island were formed along the two arc-trench systems: the western Paleo-Northeastern Japan Arc and the eastern Paleo-Kuril Arc, which collided with each other in the Paleogene (Kiminami, 1989, 2010; Kimura, 1994a; Kimura & Kusunoki, 1997). Hokkaido is composed of five tectonic belts: are the Oshima, Sorachi-Yezo, Hidaka, Tokoro and Nemuro belts from the west to the east (Kiminami, 1986; Niida, 2010; Figure 1).

The Paleo-Northeastern Japan Arc was the subduction zone of the Pacific plate into the Eurasian plate. The Oshima and Sorachi-Yezo belts that are distributed to the west of Hokkaido (Figure 1) were formed along the western Paleo-Northeastern Japan Arc, and consist of the Jurassic to Cretaceous accretionary complexes and Cretaceous forearc basin deposits (Kiminami, 1986; Kito, 1987; Takashima, Nishi, & Yoshida, 2006; Takashima, Yoshida, & Nishi, 2001). These belts extend in a north-south direction and show eastward rejuvenation (Kiminami, 1986; Figure 1). On the other hand, the Paleo-Kuril Arc was the subduction zone of the Kula or Izanagi plate to the Okhotsk plate (Kimura, 1994a; Maeda, 1990; Figure 1). The Tokoro and Nemuro belts, located to the east of Hokkaido, were formed as a part of the Paleo-Kuril Arc (Kiminami, 1986). They consist of the Upper Cretaceous to Paleogene accretionary prisms and the Upper Cretaceous to Paleogene deposits (Kiminami, 1983; Naruse, 2003). The Hidaka Belt is located between the two arcs, and contains accretionary complexes of both paleo-arcs (Komatsu, 1986; Toyoshima, Komatsu, & Shimura, 1994). It consists of the Upper Cretaceous and Paleogene accretionary complex, and volcanic and metamorphic rocks (Toyoshima et al., 1994).

The middle Eocene Urahoro Group is located in Kushiro, eastern Hokkaido, and belongs to the Nemuro belt (Figures 1 and 2). It is 735–780 m thick, contains non-marine-to-littoral clastics, and is composed of conglomerate, sandstone, siltstone and coal (Mabuti, 1962; Matsui, 1962; Sasa, 1940a, 1940b; Sato et al., 1968; Kawai, 1956). The Urahoro Group unconformably overlies the Upper Cretaceous to middle Eocene Nemuro Group, and is unconformably overlain by the upper Eocene to lower Oligocene Onbetsu Group (Mabuti, 1962; Matsui, 1962). The Urahoro Group is composed of six Formations: The Beppo, Harutori, Tenneru, Yuubetsu, Shitakara and Shakubetsu Formations in ascending stratigraphic order (Sasa, 1940a, 1940b). The Rushin Formation, which is correlated with the Beppo, Harutori and Tenneru Formations, is observed at the westernmost part of the exposure (Tanai, 1957).

The Urahoro Group crops out in two regions: the eastern Konsen-coastal and the northwestern Shiranuka-hill regions (Mabuti, 1962; Matsui, 1962; Sasa, 1940a, 1940b; Figures 1 and 2). The Quaternary deposits are located in the Kushiro Marsh, which is located between these two regions, while the subsurface survey indicated that the Urahoro Group continuously extends in the subsurface of the Kushiro Marsh (New Energy and Industrial Technology Development Organization, 1990). Consequently, the Urahoro Group was formed in a single sedimentary basin (New Energy and Industrial Technology Development Organization, 1990).

Geologic structures of the Urahoro Group, however, are significantly different between the two regions (Figure 3). In the Konsen-coastal region, the bedding strikes are 140° north and the dips are 8° to the south. Tectonic folds are not obvious in this region and NW-SE directed faults are commonly observed (Mabuti, 1962). In contrast, in the Shiranuka-hill region, the NNE-SSW oriented tectonic folds and faults occur commonly, and faults that strike in other directions (NW-SE, N-S and E-W) are also observed (Mabuti, 1962). Matsui (1962) suggested that some of these folds and faults were formed synchronously with the deposition of the Urahoro Group.

The depositional age of the Urahoro Group is estimated to be the Bartonian (middle Eocene). Based on the occurrence of macrofossils and benthonic foraminifers, Sasa (1940b) and Kaiho (1983) correlated the Urahoro Group to the lower to middle part of the Poronai Formation of the Ishikari Group from which 36.7 Ma fission track age was reported. Kimura and Tsuji (1990) demonstrated that the depositional age of the bentonite tuff bed intercalated in the Rushin Formation is 38.0 Ma, based on a determination of the zircon fission-track-age. Recently, Katagiri, Naruse, Hirata, and Hattori (2016) reported the depositional age of an acidic tuff bed intercalated in the Tenneru Formation as (39.06 ±0.23) Ma by using the U-Pb radiometric dating method.

3. Methodology

3.1. Paleomagnetism

Samples for paleomagnetic analysis were collected from 28 sites in the Urahoro Group at the Shiranuka-hill region (Figures 2 and 3). The samples were taken by hand at 25 sites, while an electric-powered core drill was used at the remaining three sites. Five to eight blocks or core samples, which were oriented with a magnetic compass, were collected from each site. All samples were cut into cylindrical specimens, 25 mm in diameter and 22 mm in length.

Natural remanent magnetizations (NRM) were measured by using a superconducting rock magnetometer (model 760R of 2G Enterprises). One or two specimens were selected from each site for pilot analysis and were subjected to progressive thermal and/or alternating-field (AF) demagnetization experiments. The demagnetization experiments were conducted until the specimens showed erratic magnetic behavior. Because more stable magnetic behaviors of NRM were observed during the thermal demagnetization experiments, progressive thermal demagnetization experiments were conducted for the remaining specimens. The direction of a characteristic remanent magnetization (ChRM), which showed a linear trend of vector-endpoints decaying toward the origin of the orthogonal-endpoint diagram, was determined from each specimen by applying principal component analysis (Kirschvink, 1980) to the liner trend composed of at least three consecutive data points. Site mean directions of the ChRMs were calculated after Fisher's (1953) method at sites with four or more specimens showing ChRMs with 5.0° or less maximum angular deviation (MAD). In this study, site mean directions with 95% confidence interval (α_{95}) less than 20° were regarded as reliable records of the ancient geomagnetic field, and were used for calculating a group mean and determining paleomagnetic polarities. Site mean directions with α_{95} larger than 20° were used only in determining its polarity.

In order to clarify magnetic mineralogy, strong-field thermomagnetic experiments with a horizontal magnetic balance and thermal demagnetization experiments of composite isothermal remanences (IRMs) were performed on selected samples. In the thermomagnetic experiments, small chips of sediment samples packed in quartz cups (5 mm in diameter and 10 mm in height) were heated to approximately 720 °C and cooled in air in magnetic field of 0.25–0.6 T. The heating and cooling rates were approximately 8 °C/min. Standard paleomagnetic specimens were used for the thermal demagnetization experiments of IRMs. Following the method of Lowrie (1990), IRMs were imparted along the orthogonal three axes of each specimen in magnetic fields of 2.5 T, 0.4 T, and 0.12 T by using a pulse magnetizer (Magnetic Measurements Ltd. MMPM-10). Stepwise thermal demagnetizations of IRMs were performed at temperatures up to 680 °C in air. Remanent magnetization was measured with a 2G Enterprises superconducting magnetometer.

3.2. Zircon U-Pb radiometric dating

Samples for U-Pb radiometric dating were taken from two tuffaceous siltstone layers, named Ht1 and Ht2, respectively (Figures 2 and 3). We collected these samples from the subsurface outcrops along the tunnels of Kushiro Submarine Coal Mine (Figure 3). Ht1 and Ht2 are intercalated in the Harutori Formation, which are interpreted to be alluvial plain deposits (Sawaki et al., 2012). Ht1 is 1.25 m thick and consists of tuffacious siltstone containing abundant coaly fragments. The sample was collected from the basal part of the bed. Ht2 is 22 cm thick and is composed of tuffaceous clay.

The zircon grains for the analysis were mounted in a resin after being separated from the rock samples by using the gravity concentration and magnetic separation techniques. In these procedures, the samples were crushed and grains of over 250 μm in diameter were removed using a sieve. After the heavy minerals were concentrated by elutriation, ferromagnetic minerals were then also removed. Heavy liquid separation was then performed by using a solution of sodium polytungstate (specific gravity = 2.9). Finally, the zircon grains were handpicked and mounted on slide glasses in epoxy resin (Specifix-20, Struers). Mounted grains were polished to expose the centers of individual grains.

Dating of zircon by U-Pb analysis was carried out using laser ablation-ICP-mass spectrometry (LA-ICPMS) with a multiple collector-ICP-MS (Nu Instruments, Wrexham, UK) equipped with a 193 nm Excimer laser ablation system (Analyte Excite 500, Teledyne Cetac, Omaha, USA) (Hattori, Sakata, Tanaka, Orihahi, & Hirata, 2017; Obayashi, Tanaka, Hatori, Sakata & Hirata, 2017). The system setup and operational conditions are summarized in Table 1. An ablation pit size of 20 μm was used throughout this study. Prior to the U-Pb isotopic analyses, both backscattered-electron (BSE) and cathodo-luminescence (CL) images were created using a scanning electron microprobe (JEOL JXA-8105). For zircon grains having clear zoning textures in the BSE or CL images, U-Pb dating was conducted on both core and rim of a grain (two or three spots were selected), otherwise one spot was chosen for each grain. Mass bias factors in the LA-ICPMS system were externally corrected by normalizing the ^{207}Pb/^{206}Pb ratio for the NIST SRM610 (0.9096; Jochum & Stoll, 2008) and ^{206}Pb/^{238}U ratio for the Nancy 91500 (0.1792; Wiedenbeck et al., 1995). In addition, the ^{206}Pb/^{238}U ratios for OD3 (^{238}U-^{206}Pb age = 32.853 ±0.016 Ma; Iwano et al., 2013; Lukács et al., 2015) were measured as a secondary standard. Overall, the average ^{238}U-^{206}Pb age of the OD3 was (32.72 ±0.23) Ma (n = 17), suggesting that the estimated ages agree with the literature values, within analytical uncertainties.

Concordia diagrams were made by using Isoplot 4.15 (Ludwig, 2012). A weighted mean value of ages of measured grains was then calculated to estimate the eruptional/depositional age of each sample. Error ranges shown in this manuscript are 95% confidence limits. Discordant data were excluded from the calculation of mean ages. When two or more concordant data were obtained from a grain and there was no significant difference between the data, the datum with the smallest error range was selected as the representative age of the grain. Error ranges of individual grains were determined according to Sakata, Hattori, and Iwano (2014) and Katagiri et al. (2016).

4. Results

4.1. Paleomagnetic analysis

Initial NRM intensities of the specimens generally ranged from 10^{-10} Am^2 to 10^{-9} Am^2, whereas all specimens from three sites (1615, 1616, and 1621) and one specimen of Sites 1509 and 1611 had initial NRM intensities of approximately 10^{-8} Am^2. Low-stability components were generally observed in the demagnetization level below 280 ºC (Figure 5 a-e). These components were regarded as viscous overprints of the recent geomagnetic field because they generally had northward and downward direction. ChRMs were isolated from specimens of nine sites after the removal of the low-stability components (Table 2). ChRMs were apparent in the range from 280 ºC to 600 ºC (Figure 5a–e and Table 2). In eight sites (1501, 1506, 1507, 1608, 1612, 1615, 1616, and 1617), four or more specimens showed ChRMs with MAD $\leq 5°$ (Table 2). Samples from Sites 1615 and 1616 provided stable behaviors of ChRMs up to 600 °C (Figure 5a–e), while those of other sites showed erratic magnetic behaviors, that is, abrupt increase of remanent intensity and erratic directional change of NRM, at higher demagnetization levels above 360-480 °C (Figure 5c–d). Other specimens also showed erratic behaviors before producing ChRMs (Figure 5f).

Out of the above eight sites, six sites (Sites 1501, 1506, 1507, 1608, 1615, and 1616) yielded site-mean directions of ChRMs with $\alpha_{95} \leq 20°$, while site means from Sites 1612 and 1617 had α_{95} exceeding 20° (Table 2). The site-mean directions of the remanent six sites exhibited an antipodal relationship with a NNE-SSW trend after tilt correction (Figure 7). The fold test based on McElhinny (1964) indicated that the ChRMs were acquired before the tilting. κ_a/κ_b (= 9.4) was larger than F_c (= 2.98), where κ_a and κ_b are concentration parameter of the overall mean direction after and before tilt correction, respectively, and F_c is the F statistic, with degrees of freedom = 10 at 95% confidence limit. The means of tilt-corrected site-mean directions from the six sites are: Declenation (D) = 37.3°, Inclination (I) = 51.5°, α_{95} = 13.9° and κ = 24.3, which is regarded as the paleomagnetic direction of the Urahoro Group.

Induced magnetization (Js) curves of samples with stable magnetic components at thermal demagnetization levels up to 600 °C (Figure 6a-b) showed inflections at around 400 °C and 580 °C during heating in air, and decay to about 620 °C (Figure 6a). The soft (< 0.12 T) and medium (0.12–0.4 T) components of composite IRMs exhibited a large decrease of IRM below 400 °C and were demagnetized at 600 °C or 620 °C and the high components (0.4–2.5 T) were demagnetized at 680 °C (Figure 6a).

Samples with erratic magnetic behaviors of NRM in high temperature demagnetization steps above approximately 400 °C (Figure 5c-f) also exhibited inflections at around 400 °C and 580 °C for Js curves during heating in air (Figure 6b, c). The three IRM components were demagnetized completely at 580 °C. An increase of Js above 550 °C was remarkable for samples with no stable component of NRM at thermal demagnetization temperatures exceeding approximately 400 °C (Figure 6c).

Results of the thermomagnetic experiments and thermal demagnetization of composite IRMs suggested that magnetite was a principal magnetic mineral. The observed inflection of Js curves at approximately 400 °C also indicated the presence of maghemite or partially-maghematized magnetite. An inversion of maghemite to hematite during heating in air occurred between 250 °C and 750 °C (Dunlop & Ozemir, 1997), which generated the decrease of Js and IRM carried by maghemite (de Boer & Dekkers, 1996). Some samples exhibited Curie temperatures of 600–620 °C (Figure

6a). The Curie temperature above 600 °C has been reported for maghemite (Dunlop & Ozemir, 1997; Gehring et al., 2009). It is therefore suggested that the ChRMs isolated in this study are carried principally by magnetite and/or maghemite. Thermal demagnetization behaviors of the hard IRM components indicated the presence of hematite for some samples (Figure 6A). The increase of Js above 500 °C on the thermomagnetic curve in air can be caused by the formation of magnetite, which is probably attributed to the thermal alteration of Fe-bearing paramagnetic minerals. Erratic magnetic behavior during thermal demagnetization in air, which makes it difficult to isolate stable magnetic components of NRM, was possibly related to the presence of such a newly formed magnetite.

4.2. U-Pb radiometric dating

Ht1: Measurements on 142 spots in 96 grains and concordant data were obtained from 71 grains (Table 3). Figure 8 shows a histogram of age distribution and a concordia diagram for all concordant data, except for the datum from grain S62, which shows an exceptionally old age (Table 3). The age data exhibited a unimodal distribution around 39 Ma with two outlier data (from grain S12 and S62) (Figure 8; Table 3). The main cluster of the distribution is composed of 69 concordant data with a weighted mean of (39.54 ±0.17) Ma (Ludwig, 2012). The outlier data of grains S12 and S62 were 43 Ma and 5063 Ma, respectively. The outlier grains were different from other grains in roundness of grain outlines and colors in the CL image (Figure 9).

Ht2: Measurements were conducted on 74 spots in 58 grains; concordant data were recorded from 36 grains (Figure 8). The age data were clustered into two groups with five outlier data. The main cluster was composed of 27 data with a weighted mean of (56.18 ±0.42) Ma. The small cluster was composed of 4 data with a weighted mean of (40.8 ±1.1) Ma. Other five outlier data were 63 Ma, 92 Ma, 252 Ma, 1746 Ma, and 1880 Ma (Figure 8; Table 4). Grains showing very old ages (1746 Ma and 1880 Ma) were clearly different from the other grains in roundness of grain outlines and colors in CL images (Figure 10).

5. Discussion

5.1. Depositional age of the Urahoro Group

Radiometric dating conducted in this study indicated that tuffaceous layers in the Urahoro Group were deposited at about 40 Ma. The calculated depositional age of Ht1 and Ht2 were (39.54 ±0.17) Ma and (40.8 ±1.1) Ma, respectively, and these are concordant to the depositional age of the tuff layer Tn1 (39.06 ±0.23 Ma) in the Tenneru Formation (Figure 4; Katagiri et al., 2016). The depositional ages of the layers were calculated as the weighted mean values of the radiometric ages of zircons except for the grains that were considered to be detrital in origin. The grains S62 and S12 of the Ht1 tuffaceous layer were interpreted to be of detrital origin, due to their old radiometric ages and abraded morphology (Figure 9; Table 3). Multimodal distribution of radiometric ages of zircon grains in the Ht2 tuffaceous layer implies that Ht2 also contained abundant zircon grains of detrital origin (Figure 8; Table 4). This interpretation was supported by variations in colors, morphologies and sizes of individual grains in CL images (Figure 10). Grains of detrital origin were excluded from the age calculation and only the grains of the younger cluster were used.

Stratigraphic relationships among the tuffaceous layers with Tn1 and layers with magnetic polarities are shown in Figure 4. The normal polarities from Sites 1501, 1506, 1507, 1608, 1612, 1616, and 1617 were correlated to the polarity chron C18n.1n, ranging from 39.6 Ma to 38.6 Ma (Ogg, 2012: Figures 3 and 11) because the Tn1 layer with an age of (39.06 ±0.23) Ma was stratigraphically intercalated in the intervals of these sites (Katagiri et al., 2016; Ogg, 2012; Figures 4 and 11). The lower reversed polarities of Site 1615 were correlated with C19r, C18r, or C18n.1r based on the ages of Ht1 (39.54 ±0.27) Ma and Ht2 (40.8 ±1.1) Ma. Thus, we suggest that the deposition of the Urahoro Group started before 39.6 Ma, which is the beginning of C18n.1n. Our depositional age estimation of the Urahoro Group does not contradict previous estimates (Kaiho, 1983; Kimura & Tsuji, 1990), but gives a much stronger constraint to the age of formation of the Urahoro Group.

5.2. Paleomagnetic direction of the Urahoro Group

The paleomagnetic direction of the Urahoro Group in the Shiranuka-hill region derived in this study was characterized by a clockwise deflected declination (Table 5). Compared with the direction of the geocentric axial dipole field (GADF) expected at the Shiranuka-hill region (D = 0° and I = 57.5°), the deflection in declination was significant (37.3 ±22.7)° while that in inclination was not significant (6.0 ±13.9)°. Fujiwara and et al. (1995) also reported a clockwise-deflected paleomagnetic direction from the Urahoro Group in the Shiranuka-hill region (Table 5). While the inclination value coincides with that of this study, the declination of Fujiwara et al. (1995) is larger than that of our study (Table 5). Because they conducted progressive demagnetization only for pilot specimens and only one treatment temperature was applied for each site (Fujiwara et al., 1995), this discrepancy is probably due to the effect of the low stability components that were not removed sufficiently by Fujiwara et al. (1995). The directional data in Fujiwara et al. (1995) were obtained by one-step heating of thermal demagnetization at 100 °C, 150 °C, or 300 °C. Our demagnetization results indicate that their demagnetization levels, especially at 100 °C and 150 °C, were too low to remove the low-stability components because ChRMs were isolated at demagnetization levels above 280 °C or more in our study (Figure 5 and Table 2). In addition, Fujiwara et al. (1995) did not get data with reversed polarity, and did not describe any demagnetization behaviors. Thus, we consider that our results are more reliable.

We compared the paleomagnetic direction of the Urahoro Group with an apparent polar wandering path (APWP) for East Asia observed by Cogné et al. (2013) in order to examine tectonic movements of terranes in the Paleo-Kuril Arc relative to East Asia. Comparing with an expected direction at the Shiranuka-hill region calculated from a 40 Ma paleopole of the APWP, our data indicate a clockwise rotation of (28.0 ±23.3)° and no significant northward translation (Table 5). It is therefore suggested that the Shiranuka-hill region was subjected to a clockwise rotation of about 29° after the formation of the Urahoro Group (*ca*. 39 Ma).

5.3. Rotational movement in the Shiranuka-hill region inferred from paleomagnetic data

Two previous studies in the Shiranuka-hill region, Fujiwara et al. (1995) and Hamano et al. (1986), reported paleomagnetic directions of the Cretaceous to early Eocene Nemuro Group underlying the Urahoro Group, and those directions exhibited a large clockwise deflection of about 70° in declination (Table 5). Here we adopted the data from Hamano et al. (1986) as a paleomagnetic direction of the Nemuro Group because the data in Fujiwara et al. (1995) contained very large errors ($\alpha95$ was 88° in maximum). The paleomagnetic samples of Hamano et al. (1986) were taken from the horizons with K-Ar and fission-track ages of 54 Ma, 52 Ma, and 47.7 Ma (Fujiwara et al., 1995; Kimura and Tsuji, 1990; Shibata et al., 1984). Compared with a 50 Ma paleopole of the APWP for East Asia (Cogné et al., 2013), their data indicated a clockwise rotation of about 62° for the Shiranuka-hill region after the deposition of the Nemuro Group. The clockwise deflected declination of the Urahoro Group was smaller than that of the Nemuro Group

(Table 5): a discrepancy between the two declinations was (33.9 ±26.4)°. This implies that the Shiranuka-hill region experienced a regional clockwise rotation of about 34° between the depositions of the Nemuro and Urahoro Groups (ca. 50 Ma to 39 Ma: Figure 12).

Fujiwara et al. (1995) also reported a paleomagnetic direction of the Onbetsu Group overlying the Urahoro Group, which exhibited no discrepancy with respect to East Asia, both in its declination and in inclination (Table 5). The paleomagnetic samples of the Onbetsu Group were collected from the lower part of the Onbetsu Group (Fujiwara et al., 1995), the depositional age of which was estimated to be the latest Eocene to early Oligocene, based on the occurrence of the benthonic foraminifera (Kaiho, 1983; 1984). According to Fujiwara & Kanamatsu (1994), the horizons sampled by Fujiwara et al. (1995) were correlated to the polarity chron C13n.r, which ranged from 35.0 to 33.7 Ma (Ogg, 2012). The paleomagnetic data from the Onbetsu Group (Table 5) infers no rotational motion of the Shiranuka-hill region after the deposition of the Onbetsu Group (*ca*. 34 Ma). This implies that the clockwise rotational motion of the Shiranuka-hill region after the formation of the Urahoro Group ceased at about 34 Ma (Figure 12). It is noteworthy that the data from the Onbetsu Group by Fujiwara et al. (1995) have a large value of α_{95}, and the discrepancy between the paleomagnetic directions of the Onbetsu and Urahoro Groups is not significant (36.6 ±51.1)°.

5.4. Bent structure in the Paleo-Kuril Arc

Paleomagnetic declinations of the Paleo-Kuril Arc are summarized in Figure 13. All terranes located west of the Kushiro marsh region exhibited clockwise rotated paleomagnetic directions, although the degree of rotation differed significantly among individual terranes. In addition to the Shiranuka-hill region, paleomagnetic directions indicating larger clockwise rotations were reported from the Tokoro and Hidaka belts, the westernmost part of the Paleo-Kuril Arc (Fujiwara et al., 1995; Figure 13, Table 5). In contrast, paleomagnetic directions of the Nemuro Group from the eastern part of the Paleo-Kuril Arc, namely the Konsen-coastal region, suggest that tectonic blocks east of the Kushiro marsh region did not experience rotation after the formation of the Nemuro Group (Fujiwara & Kanamatsu, 1990; Nifuku, Kodama, Shigeta & Naruse, 2009; Tanaka & Uchimura, 1989; Figure 13, Table 5). These paleomagnetic data imply that the western wing of the curved tectonic belt consist of some clockwise rotated terranes while the eastern part is a non-rotated block (Figure 13). The boundary between the western and eastern block was inferred to be in the Kushiro marsh region.

Geophysical data of the Paleo-Kuril Arc also imply that a large block boundary of the Paleo-Kuril Arc was located in the Kushiro mash region (Figure 13). The gravity survey results of Yamamoto and Matsushima (1990) reveal that a positive gravity anomaly, corresponding to the distribution of the Nemuro and Urahoro Groups, extends east to west in the Konsen-coastal region, while the trend of the anomaly turns at the Kushiro marsh region and extends north to south in the Shiranuka-hill region. The Urahoro Magnetic Anomaly Belt, which corresponds to the distribution of ultramafic rocks in the Nemuro Group, was also bent offshore Kushiro (Ogawa & Sunakawa, 1976; Figure 13). These geophysical data indicate that the entire tectonic block distributed west of the Kushiro marsh region experienced a clockwise rotation or northward migration relative to the Konsen-coastal region, resulting in the bent structure of the Paleo-Kuril Arc.

5.5. Arc-Arc collision as a cause of the bent structure in the Paleo-Kuril Arc terranes

This study suggests a clockwise rotation of 29° for the Shiranuka-hill region after the deposition of the Urahoro Group (*ca*. 39 Ma). This implies that the clockwise rotational motion was initiated before the deposition of the Urahoro Group (*ca*. 50 Ma), and a clockwise rotation of about 34° occurred between 50 Ma and 39 Ma. The rotational motion in the Shiranuka-hill region possibly ceased before the formation of the Onbetsu Group (*ca*. 34 Ma).

The timing of the rotational motion for the Shiranuka-hill region between 50 Ma and 39 Ma suggests that the block rotation occurred due to the arc-arc collision between the Paleo-Kuril Arc and the Paleo-Northeastern Japan Arc. Previous studies have suggested that the region rotated due to the opening of the back-arc basin (the Kuril Basin) of the Kuril Arc (Fujiwara & Kanamatsu, 1994; Fujiwara et al., 1995). However, the rotational motion in the region before 39 Ma contradicts this hypothesis because the oldest estimate for the initiation of spreading of the Kuril Basin was during the Oligocene, 34 Ma. Iijima and Tada (1990) and Fukusawa and Ishihara (1992) concluded that the Kuril Basin was formed synchronously with the deposition of the Takkobu Formation, during the upper Oligocene to the lower Miocene. Maeda (1990) suggested that the Kuril basin opened just after 16 Ma based on the cessation of the Hidaka metamorphism and the coeval north-south trending extension. Kimura and Tamaki (1985) estimated that the Kuril Basin was formed during the Oligocene to middle Miocene by comparing the basal depth and heat flow of the Kuril Basin with those of the Shikoku Basin and South China Sea. Accordingly, the rotation of the Shiranuka-hill region before 39 Ma cannot be attributed to the spreading of the Kuril Basin.

The rotation age estimated by this study is concordant with the timing of the initiation of the arc-arc collision, which has been deduced from the transition of sedimentary basins (Iijima, 1996; Kiminami, 2010; Kimura & Kusunoki, 1997). In Hokkaido Island, the Paleogene strata, including the Urahoro Group, are characterized by coal-bearing sub-aerial deposits with gravels supplied from the trenchside (Iijima, 1996; Nagahama, Terui, Nagahama, & Sato, 1978). These features are in contrast to those of the underlying Upper Cretaceous forearc deposits, including the Nemuro Group, which mainly consist of fine-grained marine deposits supplied from each paleo-arc zones (Naruse, 2003; Takashima et al., 2001; Takashima, Kawabe, Nishi, Moriya, Wani & Ando, 2004). It has been suggested that the arc-arc collision occurred just before the late Eocene on the basis of drastic changes in sedimentological features in the basins, as well as the cessation of magmatism along the eastern margin of the Eurasian plate (Iijima, 1996; Kiminami, 2010; Kimura & Kusunoki, 1997). Kimura and Kusunoki (1997) suggested that the collision occurred before the back-arc spreading, and our result supports this view. Therefore, we suggest that the Shiranuka-hill region was rotated due to the oblique arc-arc collision of the Paleo-Kuril Arc and Paleo-Northeastern Japan Arc, which is a common cause of block rotations of terranes (e. g. Kano, 2002; Takahashi & Saito, 1997).

6. Conclusions

Radiometric dating, using U-Pb, of zircons extracted from tuffaceous beds, and paleomagnetic analysis in the Urahoro Group, were conducted in this study. Based on the U-Pb ages, the depositional age of the Urahoro Group was estimated to be approximately 39 Ma. A paleomagnetic direction of the Urahoro Group in the Shiranuka-hill region indicated a 29° clockwise rotation of the region after its deposition (*ca*. 39 Ma). In conjunction with previous paleomagnetic data, our data indicated that the Shiranuka-hill region experienced an approximately 34° clockwise rotation between the deposition of the Nemuro and Urahoro Groups (50–39 Ma) and 37° clockwise rotation between the deposition of the Urahoro and Onbetsu Groups (39–34 Ma). The clockwise rotational motion of the Shiranuka-hill region is probably representative of the block rotation of the western part of the Paleo-Kuril Arc, resulting in the formation of the bent structure of the arc in the eastern Hokkaido Island. The age constraints of the block rotation revealed in this study contradict the conventional hypothesis that the block rotation of the Paleo-Kuril Arc was formed by the opening of the Kuril basin. Rather, our study supports the hypothesis that the collision between the Paleo-Kuril Arc and Paleo-Northeastern Japan Arc caused the rotation of the tectonic blocks in the Paleo-Kuril Arc.

Acknowledgements

Measurements of paleomagnetism and radiometric ages were conducted at Kyoto University. We wish to thank Harutaka Sakai, Tetsu Kogiso, and Tetsuo Kawakami who kindly let us use laboratory equipment for the radiometric dating. Thanks are also due to Kota Takatsuka and Hideyuki Obayashi for their support in using the JOEL JXA-8105 superprobe, and ICP-MS, respectively. We also thank Naoyoshi Hasegawa of Shiranuka village, Takaori Ishikawa of the Kushiro museum, Katsumi Uchida and Yoshihiro Ito of the Kushiro Coal Mine and all the members of the Akkesi Marine Station for supporting us during the field survey in Kushiro. We appreciate helpful reviews by Tetsuji Muto, Gaku Kimura and Koji Uno. We would like to thank Serem Gideon Kiptoo of INPEX and Editage (www.editage.com) for English language editing. This work was supported by JSPS KAKENHI Grant Numbers JP26610161 and JP26287127.

References

Beck, Jr. M. E. (1980). Paleomagnetic record of plate‐margin tectonic processes along the western edge of North America. *Journal of Geophysical Research: Solid Earth*, **85**(B12), 7115–7131.

Cogné, J.-P., Besse, J., Chen, Y., & Hankard, F. (2013). A new Late Cretaceous to Present APWP for Asia and its implications for paleomagnetic shallow inclinations in Central Asia and Cenozoic Eurasian plate deformation. *Geophysical Journal International*, **192**(3), 1000–1024.

de Boer, C. B., & Dekkers, M. J. (1996). Grain-size dependence of the rock magnetic properties for a natural maghemite, *Geophysical Research Letters*, **23**(20), 2815–2818.

Duermeijer, C. E., Nyst, M., Meijer, P. T., Langereis, C. G., & Spakman, W. (2000). Neogene evolution of the Aegean arc: paleomagnetic and geodetic evidence for a rapid and young rotation phase. *Earth and Planetary Science Letters*, **176**(3-4), 509-525.

Dunlop, D. J., & Özdemir, Ö. (2001). *Rock magnetism: fundamentals and frontiers* (Vol. 3). Cambridge, England: Cambridge university press.

Fisher, R. A. (1953). Dispersion on a sphere. *Proceedings of the Royal Society of London. Series A. Mathematical and Physical Sciences*, **217**(1130), 295–305.

Fujiwara, Y., & Kanamatsu, T. (1990). Magnetostratigraphy of the Nemuro Group, east Hokkaido, Japan. *Rock Magnetism and Paleogeophysics*, **17**, 38–41.

Fujiwara, Y., & Kanamatsu, T. (1994). On the age of bending structure in eastern Hokkaido. *Chishitsu News*, **34**, 283–291. (in Japanese).

Fujiwara, Y., Kanamatsu, T., & Nanayama, F. (1995). Tectonic evolution of two paleo arc-trench systems in Hokkaido, northern Japan. *Gepfisica International.*, **478**, 45–48.

Fukusawa, H., & Ishihara, C. (1992). Preliminary report on the first appearance of nutrient-rich deep water in inner zone of the Kuril Arc. *Journal of the Sedimentological Society of Japan*, **37**(37), 21–30. (in Japanese with English abstract and captions).

Gehring, A. U., Fischer, H., Louvel, M., Kunze, K., & Weidler, P. G. (2009). High temperature stability of natural maghemite: a magnetic and spectroscopic study. *Geophysical Journal International*, **179**(3), 1361–1371.

Hamano, Y., Tsunakawa, H., Saito, Y., & Kikawa, E. (1986). Paleomagnetism of the eastern Hokkaido. *Chikyu monthly*, **8**, 434–438. (in Japanese).

Hattori, K., Sakata, S., Tanaka, M., Orihashi, Y., & Hirata, T. (2017). U-Pb age determination for zircons using laser ablation-ICP-mass spectrometry equipped with six multiple-ion counting detectors. *Journal of Analytical Atomic Spectrometry*, **32**(1), 88–95.

Hoyanagi, K., & Miyasaka, S. (2010). Kushiro coal field and Kitami region. In Geological Society of Japan (Eds.), *Monograph on Geology of Japan*, Vol. 1: Hokkaido (pp. 109–112). Tokyo, Japan: Asakura Publ. (in Japanese).

Iijima, A. (1996). Evolution of the Paleogene Sedimentary Basins in Hokkaido. *Journal of Geography (Chigaku Zasshi)*, **105**, 178–197. (in Japanese with English abstract and captions).

Iijima, A., & Tada, R. (1990). Evolution of Tertiary sedimentary basins of Japan in reference to opening of the Japan

Sea. *Journal of the Faculty of Science. University of Tokyo, Section 2: Geology, Mineralogy, Geography, Geophysics*, **22**, 121–171.

Iwano, H., Orihashi, Y., Hirata, T., Ogasawara, M., Danhara, T., Horie, K., Hasebe, N., Sueoka, S., Tamura, A., Hayasaka, Y., Katsube, A., Ito, H., Tani, K., Kimura, J.-I., Chang, Q., Kouchi, Y., Haruta, Y., & Yamamoto, K. (2013). An inter-laboratory evaluation of OD-3 zircon for use as a secondary U–Pb dating standard. *Island Arc*, **22**, 382–394.

Jochum, K. P., & Stoll, B. (2008). Reference materials for elemental and isotopic analyses by LA-(MC)-ICP-MS: successes and outstanding needs. In P. J. Sylvester, (Ed.), Laser ablation ICP-MS in the Earth sciences: Current practices and outstanding issues. *Mineralogical Association of Canada*, 147–168. Vancouver, BC: Mineralogical Association of spiepr132 Canada.

Kaiho, K. (1983). Geologic ages of the Paleogene of Hokkaido, Japan based upon planktonic foraminifera -The relationship between the hiatuses and sea-level movements-. *fossils*, **34**, 41–49. (in Japanese with English abstract and captions).

Kaiho, K. (1984). Upper Cretaceous to Paleogene foraminiferal biostratigraphy in the Shiranuka area, eastern Hokkaido. *Biostratigraphy and international correlation of the Paleogene System of Japan, Yamagata University, Yamagata*, 35–48.

Kanamatsu, T., Nanayama, F., Iwata, K., & Fujiwara, Y. (1992). Pre-Tertiary Systems on the western side of the Abashiri Tectonic Line in the Shiranuka area, eastern Hokkaido, Japan: Implications to the tectonic relationship between the Nemuro and Tokoro Belts. *Journal of the Geological Society of Japan*, **98**(12), 1113–1128. (in Japanese with English abstract and captions).

Kano, K. (2002). Re-arrangement of the shallow-level structure of Southwest Japan Arc due to the collision of the Izu-Bonin Arc. Bull. Earthq. *Bulletin of the Earthquake Research Institute, University of Tokyo*, **77**, 231–248. (in Japanese with English abstract).

Katagiri, T., Naruse, H., Hirata, T., & Hattori, K. (2016). U – Pb age of the tuff bed in the Urahoro Group, eastern Hokkaido, northern Japan. *Journal of the Geological Society of Japan*, **122**, 495–503. (in Japanese with English abstract and captions).

Kawai, M. (1956). Explanatory text of the geological map of Japan, "Konbumori". Scale 1:50,000. Hokkaido, Japan: Hokkaido Development Agency, 59+8p (in Japanese with Englishabstract).

Kiminami, K. (1983). Sedimentary history of the Late Cretaceous-Paleocene Nemuro Group, Hokkaido, Japan: A forearc basin of the Paleo-Kuril arc-trench system. *Journal of the Geological Society of Japan*, **89**, 607–624.

Kiminami, K. (1986). Cretaceous tectonics of Hokkaido and the environs of the Okhotsk Sea. *Monograph of the Association for the Geological Collaboration in Japan,* **31**, 403–418. (in Japanese with English abstract and captions).

Kiminami, K. (1989). Some new propositions concerning the tectonics around Hokkaido. *Chikyu monthly*, **11**, 309–315. (in Japanese).

Kiminami, K. (2010). Latest Cretaceous to Paleogene. In Geological Society of Japan (Eds.), *Monograph on Geology* *of Japan*, Vol. 1: Hokkaido (pp. 526–528). Tokyo, Japan: Asakura Publication (in Japanese).

Kimura G. (1990). What setting is for the crustal flow in the Hidaka? *Chikyu monthly*, **12**, 445–453. (in Japanese).

Kimura, G. (1993) Cenozoic Tectonics in Hokkaido. 100 Anniversary of Geology in Japan, 220–225. (in Japanese).

Kimura, G. (1994a). The latest Cretaceous-early Paleogene rapid growth of accretionary complex and exhumation of high pressure series metamorphic rocks in northwestern Pacific margin. *Journal of Geophysical Research: Solid Earth*, **99**(B11), 22147–22164.

Kimura, G., & Kusunoki, K. (1997). The Hidaka Orogeny and tectonics of arc-arc junction. *Memoirs of the Geological Society of Japan* , **47**, 295–305. (in Japanese with English Abstract).

Kimura, K., & Tsuji, Y. (1990). Research about the formation and development of sedimentary basin. *Ann. Rept. TRC's Act.*, 10–14. (in Japanese).

Kirschvink, J. L. (1980). The least-squares line and plane and the analysis of palaeomagnetic data. *Geophysical Journal International*, **62**, 699-718.

Kito, N. (1987). Stratigraphic relation between greenstones and clastic sedimentary rocks in the Kamuikotan Belt, Hokkaido, Japan. *Journal of the Geological Society of Japan*, **93**, 21–35. (in Japanese with English Abstract).

Klootwijk, C. T., Conaghan, P. J., & Powell, C. M. (1985). The Himalayan Arc: large-scale continental subduction, oroclinal bending and back-arc spreading. *Earth and Planetary Science Letters*, **75**(2-3), 167-183.

Komatsu, M., Miyashita, S., & Arita, K. (1986). Composition and structure of the Hidaka metamorphic belt, Hokkaido—historical review and present status. *Monograph of the Association for the Geological Collaboration* *in Japan*, **31**, 189-203.

Ludwig, K.R. (2012). User’s Manual for A Geochronological Toolkit for Microsoft Excel Berkeley Geochronology Center. *A Geochronology Center Special Publication.*

Lukács, R., Harangi, S., Backmann, O., Guillong, M., Danišík, M., Buret, Y., Albrecht, Q. von, Dunkl, I., Fodor, L., Sliwinski, J., Soós, I., & Szepesi, J. (2015). Zircon geochronology and geochemistry to constrain the youngest eruption events and magma evolution of Mid-Miocene ignimbrite flare-up in the Pannonian Basin, eastern-central Europe. *Contributions to Mineralogy and Petrology*, **170**(5-6), 52.

Mabuti, S. (1962). Sedimentological and structural study of the Tertiary Kushiro coal field. *Doctoral disseertation of Tohoku University*, **56**, 1–42. (in Japanese with English abstract).

McCabe, R. (1984). Implications of paleomagnetic data on the collision related bending of island arcs. *Tectonics*, **3**, 409–428.

Maeda, J. (1990). Opening of the Kurd Basin deduced from the magmatic history of Central Hokkaido, North Japan. *Tectonophysics*, **174**, 235–255.

Matsui, M. (1962). Sedimentological study of the Paleogene basin of Kushiro in Hokkaido, Japan. *Journal of the Faculty of Science, Hokkaido University. Series 4, Geology and mineralogy*, **11**(3), 431–480.

Nagahama, H., Terui, K., Nagahama, Y., & Sato, M. (1978). Sediment source of the Urahoro Group induced from cross beddings and gravels. *85th Annual Meeting of Geological Society of Japan, Abstract*, 200. (in Japanese)

Nakanishi, A., Kurashimo, E., Tatsumi, Y., Yamaguchi, H., Miura, S., Kodaira, S., Obana, K., Takahashi, N., Tsuru, T., Kaneda, Y., Iwasaki, T., & Hirata, N. (2009). Crustal evolution of the southwestern Kuril Arc, Hokkaido Japan, deduced from seismic velocity and geochemical structure. *Tectonophysics,* **472**(1-4), 105-123.

Nanayama, F. (1992). Stratigraphy and facies of the Paleocene Nakanogawa Group in the southern part of central Hokkaido, Japan. *Journal of the Geological Society of Japan* , **98**, 1041-1059. (in Japanese with English abstract and captions).

Nanayama, F., Kanamatsu, T., & Fujiwara, Y. (1993). Sedimentary petrology and paleotectonic analysis of the arc—arc junction: the Paleocene Nakanogawa Group in the Hidaka Belt, central Hokkaido, Japan. *Palaeogeography, palaeoclimatology, palaeoecology*, **105**(1–2), 53–69.

Naruse, H. (2003). Cretaceous to Paleocene depositional history of North-Pacific subduction zone: Reconstruction from the Nemuro Group, eastern Hokkaido, northern Japan. *Cretaceous Research,* **24**(1), 55–71.

New energy And Industrial Technology Department Organization (1990). Basic survey for the exploer of coal. *Report of a boring survey 4-1 at offshore Kushiro*. (in Japanese).

Nifuku, K., Kodama, K., Shigeta, Y., & Naruse, H. (2009). Faunal turnover at the end of the Cretaceous in the North Pacific region: Implications from combined magnetostratigraphy and biostratigraphy of the Maastrichtian Senpohshi Formation in the eastern Hokkaido Island, northern Japan. *Palaeogeography, palaeoclimatology, palaeoecology*, **271**, 84–95.

Niida, S. (2010). Geologic abstract and subdivision of Hokkaido, In Geological Society of Japan (Eds.), *Monograph on Geology of Japan*, Vol. 1: Hokkaido (pp. 13–15). Tokyo, Japan: Asakura Publication (in Japanese)

Obayashi, H., Tanaka, M., Hattori, K., Sakata, S., & Hirata, T. (2017). In-situ 207Pb/206Pb isotope ratio measurement using Dual-Daly Ion Counting ICP-Mass Spectrometer. *Journal of Analytical Atomic Spectrometry*, **32**(3), 686–691.

Ogasawara, M., Shibata, K., & Uchiumi, S. (1998). K-Ar ages and petrological characteristics of granitoid pebbles from the Eocene Beppo Formation in the Kushiro region, Hokkaido, Japan. *Journal of the Geological Society of Japan*, **104**, 516–524. (in Japanese with English abstract and captions).

Ogawa, K., & Suyama, J. (1976). Disribution of Aeromagneic Anomalies, Hokkaido, Japan and its Geological Implication, In Aoki, H., Iizuka, S. (Eds.), *Volcaoes and Tectonosphere* (pp. 207–215) . Kanagawa, Japan: Tokai University Press.

Ogg, J. G. (2012). Geomagnetic polarity time scale, In Gradstein, F. M., Ogg, J. G., Schmitz, M. D., Ogg, G. M. (Eds.), *The geologic time scale 2012* (pp. 85–113). Elsevier, Oxford.

Otofuji, Y. (1996). Large tectonic movement of the Japan Arc in late Cenozoic times inferred from paleomagnetism: Review and synthesis, *Island Arc*, **5**, 229-249.

Otofuji, Y. I., Enami, R., Yokoyama, M., Kamiya, K., Kuma, S., Saito, H., & Matsuda, T. (1999). Miocene clockwise rotation of southwest Japan and formation of curvature of the Median Tectonic Line: Paleomagnetic implications. *Journal of Geophysical Research: Solid Earth*, **104**(B6), 12895-12907.

Sakata, S., Hattori, K., & Iwano, H. (2014). Determination of U – Pb Ages for Young Zircons using Laser Ablation-ICP-Mass Spectrometry Coupled with an Ion Detection Attenuator Device. *Geostandards and Geoanalytical*

Research, **38**, 409–420.

Sasa, Y. (1940a). Stratigraphy of the Tertiary deposits in the Kushiro coal field and a critical review of the opinions expressed.a. *Journal of Hokkaido Coal Mine Association*, **307**, 1–19. (in Japanese)

Sasa, Y. (1940b). Stratigraphy of the Tertiary deposits in the Kushiro coal field and a critical review of the opinions expressed.b. *Journal of Hokkaido Coal Mine Association*, **308**, 1–24. (in Japanese).

Sato, S., Nobata, H., Sato, M., Higashi, T., Inoye, A., & Kanazawa, T. (1968). The results of the geologic survey and test drilling of the submarine coal field in Taiheiyo Tanko. *Mining Geol*ogy, **18**, 173–184. (in Japanese with English Abstract).

Sawaki, T., Nakajima, T., Ogasawara, M., Suzuki, Y., Tanahasji, M., Kaneko, M., Kadosawa, N., & Nakanishi, T. (2012). Outcrops of the Urahoro Group along the Kushiro Coast, Hokkaido. *Chishitsu News*, **1**, 363–368. (in Japanese).

Shibata, K., Uchiumi, S., Uto, K., & Nakagawa, T. (1984). K-Ar age results 2, New data from the Geological Survey of Japan. *Bulletin of the Geological Survey of Japan,* **35**, 331–340. (in Japanese with English Abstract).

Takahashi, M., & Saito, K. (1997). Miocene intra-arc bending at an arc-arc collision zone , central Japan. *Island Arc*, **6**, 168–182.

Takashima, R., Kawabe, F., Nishi, H., Moriya, K., Wani, R., & Ando, H. (2004). Geology and stratigraphy of forearc basin sediments in Hokkaido, Japan: Cretaceous environmental events on the north-west Pacific margin. *Cretaceous Research*, **25**(3), 365–390.

Takashima, R., Nishi, H., & Yoshida, T. (2006). Late Jurassic–Early Cretaceous intra-arc sedimentation and volcanism linked to plate motion change in northern Japan. *Geological Magazine*, **143**, 753–770.

Takashima, R., Yoshida, T., & Nishi, H. (2001). Stratigraphy and sedimentary environments of the Sorachi and Yezo Groups in the Yubari-Ashibetsu area, Hokkaido, Japan. *Journal of the Geological Society of Japan*, **107**(6), 359–378. (in Japanese with English abstract and captions).

Tanai, M. (1957). *Geological Map of Onbetsu Prefecture, Scale 1: 50,000 and its Explanatory Text*. Hokkaido. Regional Development Bureau. (in Japanese).

Tanaka, H., & Uchimura, H. (1989). Tectonics of Hokkaido from Paleomagnetism. *Chikyu monthly*., **11**, 298–306. (in Japanese).

Toyoshima, T., Komatsu, M., & Shimura, T. (1994). Tectonic evolution of lower crustal rocks in an exposed magmatic arc section in the Hidaka metamorphic belt, Hokkaido, northern Japan. *Island Arc*, **3**(3), 182-198.

Weil, A. B., Van der Voo, R., & van der Pluijm, B. A. (2001). Oroclinal bending and evidence against the Pangea megashear: The Cantabria-Asturias arc (northern Spain). *Geology*, **29**(11), 991-994.

Wiedenbeck, M., Alle, P., Corfu, F., Griffin, W.L., Meier, M., Oberli, F., Von quadt, A., Roddick, J.C., & Spiegel, W. (1995). Three natural zircon standards for U-Th-Pb, Lu-Hf, trace element and Ree analysis. *Geostandards newsl*etter, **19**(1), 1–23.

Yamamoto, A., & Matsushima, T. (1990). Gravit anormally and subsurface structure of Tokachi plains. *Chikyu monthly*, **12**, 566–570. (in Japanese).

567

Figure Captions

Figure 1. Geographic map of the Northwestern Pacific Region (a) and Geotectonic division of Hokkaido Island (b), modified after Nakanishi et al. (2009) and Nida (2010). Hokkaido is located at the convergent boundary and consists of western Paleo-Northeastern Japan Arc and eastern Paleo-Kuril Arc.

Figure 2. Conventional tectonic model of Hokkaido based on Fujiwara and Kanamatsu (1994), Kiminami (2010, 1989), Kimura (1994a), Kimura and Kusunoki (1997). (a) Two arc-trench systems were formed. (b) The arcs collided with each other. (c) The spreading of the Kuril basin caused a transpressional tectonic condition at the boundary of the two arcs, resulting in the clockwise rotation of the Shiranuka-hill region. (d) Hidaka Orogeny occurred due to westward migration of the Kuril forearc sliver.

Figure 3. Maps showing sampled locations. (a, b) Geological map of pre-Neogene terranes in Kushiro with sites of the U-Pb radiometric dating. Modified after Sato et al. (1976), Yamaguchi et al. (1971) and https://gbank.gsj.jp/datastore/. (c–g) Locations of paleomagnetic sampling.

Figure 4. Stratigraphic relationships of horizons of the radiometric and paleomagnetic samples. Geological columns of the western region were made from a route map along the Satombetsu river section (Figure 3d). Columns of the eastern region were made from Miyasaka and Hoyanagi (2010). Black and white circles indicate normal and reversed

paleomagnetic polarities, respectively.

Figure 5. Examples of progressive demagnetization results displayed on orthogonal-endpoint diagrams. Polygonal lines with solid and open circles are on the horizontal and north-south vertical planes, respectively. Div., intensity of remanence for a division on axes of the orthogonal-endpoint diagrams (Am^2).

Figure 6. Typical results of strong-field thermomagnetic (left) and thermal demagnetization experiments of composite IRMs (right) for selected samples.

Figure 7. Equal-area plots of site mean directions from the Urahoro Group in the Shiranuka-hill region before and after tilt corrections. Solid and open symbols are on the lower and upper hemispheres, respectively. Ovals around the directions are 95% confidence limits. Numerals indicate site numbers.

Figure 8. U-Pb ages for zircons in the tuffaceous layers in the Urahoro Group. (a) Histogram of all U-Pb radiometric age of individual grains obtained from Ht1, except for one exceptionally old age datum from grain S62. (b) Concordia plot of all concordant data except for the age obtained from grain S62. (c) Histogram of all concordant data obtained from Ht2. (d) Concordia plot of concordant data except for the clusters of 92 Ma, 252 Ma, 1746 Ma, and 1880 Ma.

Figure 9. CL images of representative zircon grains from Ht1. Measured points are shown with their 206Pb/238U ages. Grains with relatively young, medium and old ages are shown by the upper, middle and lower lines, respectively. Scale bars are 20 μm long.

Figure 10. CL images of representative zircon grains obtained from Ht2. Measured points are shown with their ^{206}Pb/^{238}U ages. Scale bars are 20 μm long.

Figure 11. Correspondence of ages of tuffaceous beds with the geomagnetic polarity timescale of Ogg (2012).

Figure 12. Paleomagnetic data in the Shiranuka-hill region. (a) Equal-area plots of paleomagnetic directions from the Nemuro, Urahoro and Onbetsu Groups (Fujiwara et al., 1995; Hamano et al., 1986). (b) Paleomagnetic declinations from the three groups, with 95% confidence limit, as a function of the depositional ages of the groups.

Figure 13. Distribution of terranes belonging to the Paleo-Kuril Arc (modified after Niida, 2010) and paleomagnetic declinations from the terrane with 95% confidence limits (Fujiwara et al., 1995; Fujiwara & Kanamatsu; 1990; Hamano et al., 1986; Nifuku et al., 2009). Yusenkyo Fm. was deposited in late Campanian–early Maastrichtian (Kanamatsu et al., 1992) and Kamitoyoni Fm. was deposited in the late Cretaceous to Paleocene (Nanayama, 1992).

Fm., Formation. G., Group.

Table 1. Instrumentation and operational settings of the LA-ICP-MS technique for U-Pb dating.

Table 2. Paleomagnetic data from the Urahoro Group.

Footnotes: Lat, latitude (N°); Long, longitude (E°); n_A, number of specimens used in calculation of the site mean direction; n, number of samples collected from a site. D_{IS}, I_{IS}: *in-situ* declination and inclination, respectively; D_{TC}, I_{TC}, declination and inclination, respectively, after tilt correction and true north correction; N, normal polarity; R, reversed polarity; －, No data.

Table 3. Calculated $^{207}Pb/^{235}U$ and $^{206}Pb/^{238}U$ ages of zircon grains from Ht1.

Footnotes: 7/5 Age, $^{207}Pb/^{235}U$ age (Ma); 6/8 Age, $^{206}Pb/^{238}U$ age (Ma). Uncertainties are reported at the 2σ level. Data with circles in the left column were used for calculation of the mean.

Table 4. Calculated $^{207}Pb/^{235}U$ and $^{206}Pb/^{238}U$ ages of zircon grains from Ht2.

Footnotes: 7/5 Age, $^{207}Pb/^{235}U$ age (Ma); 6/8 Age, $^{206}Pb/^{238}U$ age (Ma). Uncertainties are reported at the 2σ level. Data with circles in the left column were used calculation of the mean.

Table 5. Paleomagnetic directions obtained from the Paleo-Kuril Arc.

Footnotes: D and I, tilt-corrected declination and inclination of the observed mean directions, respectively; ΔD and ΔI, 95% confidence limit of declination and inclination, respectively. $\Delta D = \sin^{-1}(\sin(\alpha95)/\cos(I))$, $\Delta I = \alpha95$; n, number of data points used in calculating mean directions; R and F, discrepancies in declination (R) and inclination (F) between the observed and expected directions; ΔR and ΔF, 95% confidence limits of R and F, respectively. Tectonic parameters were calculated based on the definition of Beck et al. (1980); －, no data; R. P., reference pole of East Asia from Cogné et al. (2013). Paleomagnetic directions and paleomagnetic pole positions of the previous studies, except for Hamano et al. (1986), were recalculated from site-mean directions with $\alpha95 \leqq 20$. The positions of sampling sites A-E in Fujiwara and Kanamatsu (1990) were assumed as follows: A, 43.05°N, 144.84°E; B, 43.14°N, 145.18°E; C, 43.15°N, 145.16°E; D, 43.19°N, 145.53°E; E43.15°N, 145.23°E.

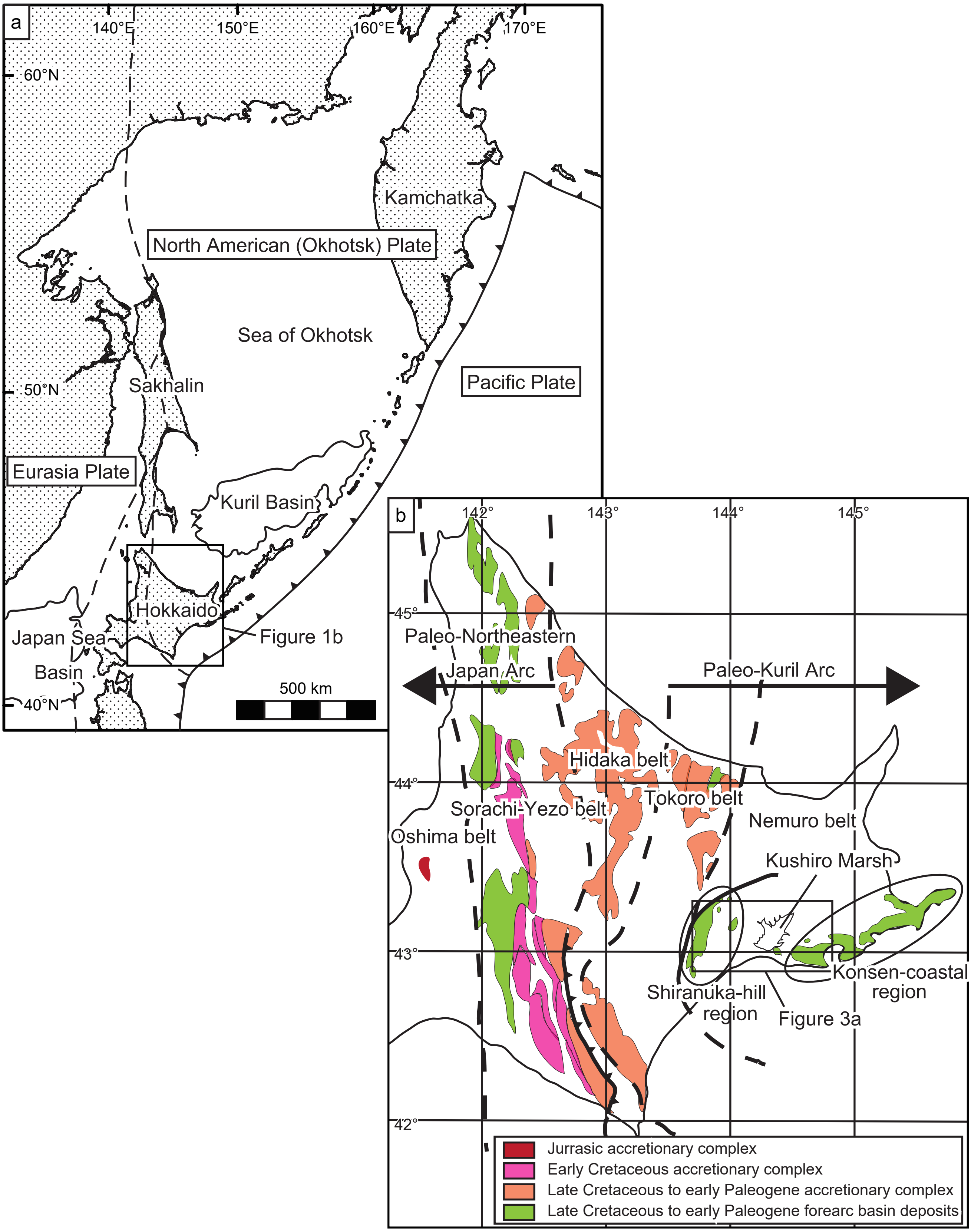

Figure 1. Geographic map of the Northwestern Pacific Region (a) and Geotectonic division of Hokkaido Island (b), modified after Nakanishi et al. (2009) and Nida (2010). Hokkaido is located at the convergent boundary and consists of western Paleo-Northeastern Japan Arc and eastern Paleo-Kuril Arc.

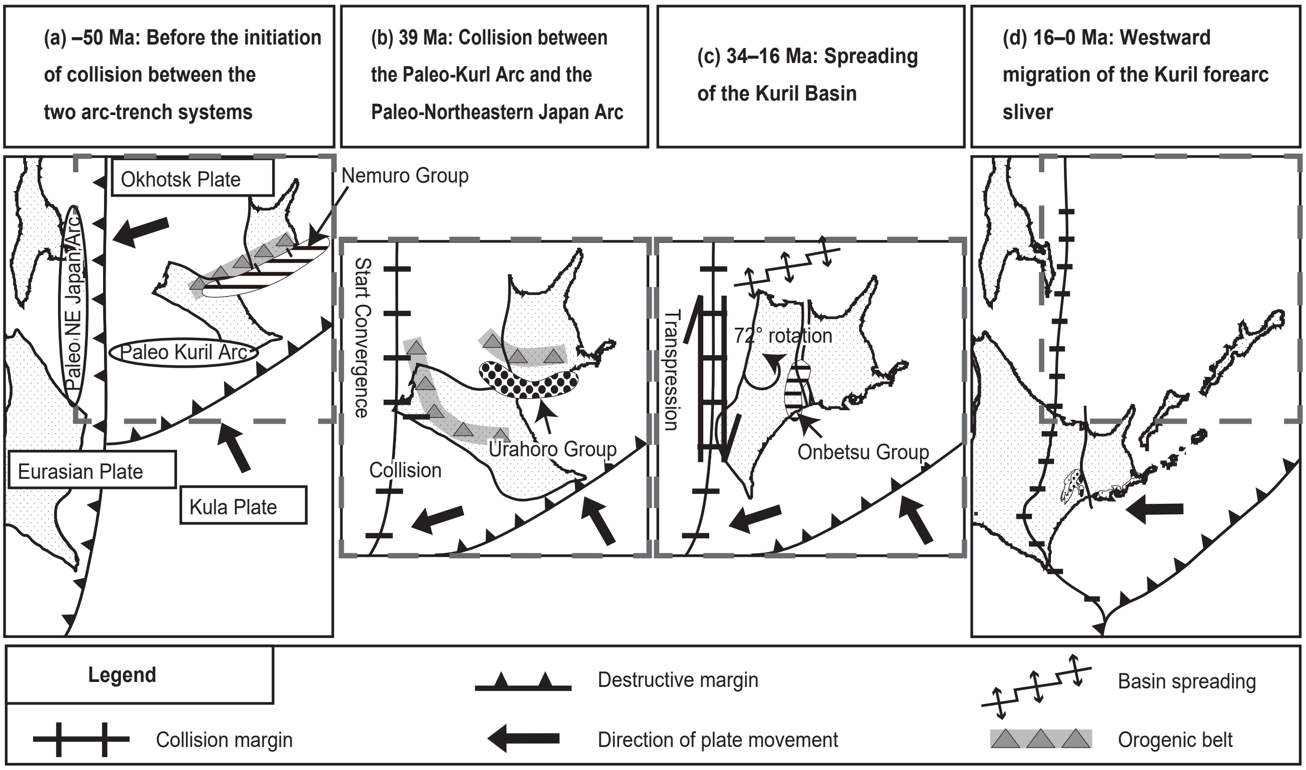

Figure 2. Conventional tectonic model of Hokkaido based on Fujiwara and Kanamatsu (1994), Kiminami (2010, 1989), Kimura (1994a), Kimura and Kusunoki (1997). (a) Two arc-trench systems were formed. (b) The arcs collided with each other. (c) The spreading of the Kuril basin caused a transpressional tectonic condition at the boundary of the two arcs, resulting in the clockwise rotation of the Shiranuka-hill region. (d) Hidaka Orogeny occurred due to westward migration of the Kuril forearc sliver.

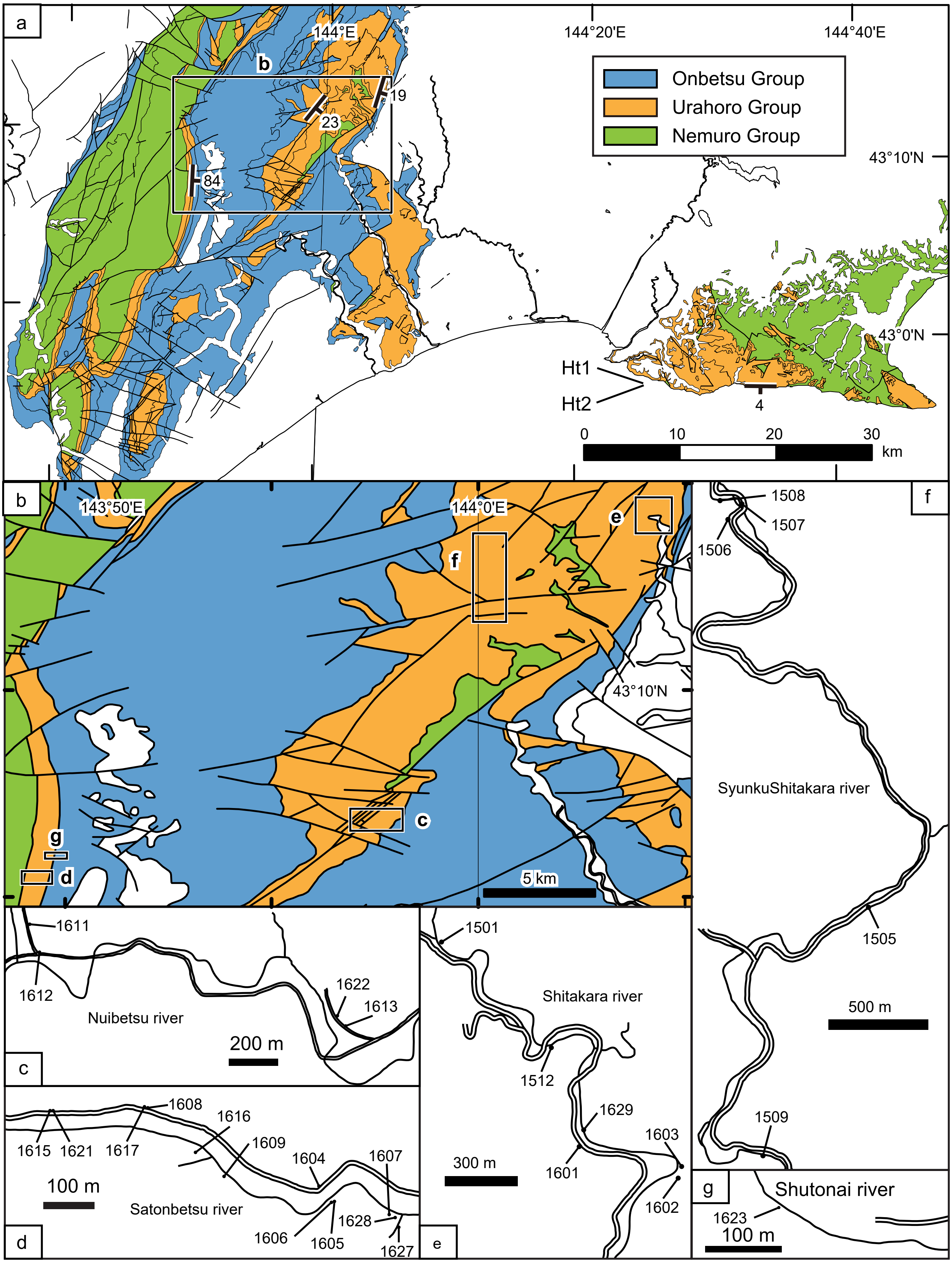

Figure 3. Maps showing sampled locations. (a, b) Geological map of pre-Neogene terranes in Kushiro with sites of the U-Pb radiometric dating. Modified after Sato et al. (1976), Yamaguchi et al. (1971) and https://gbank.gsj.jp/datastore/. (c–g) Locations of paleomagnetic sampling.

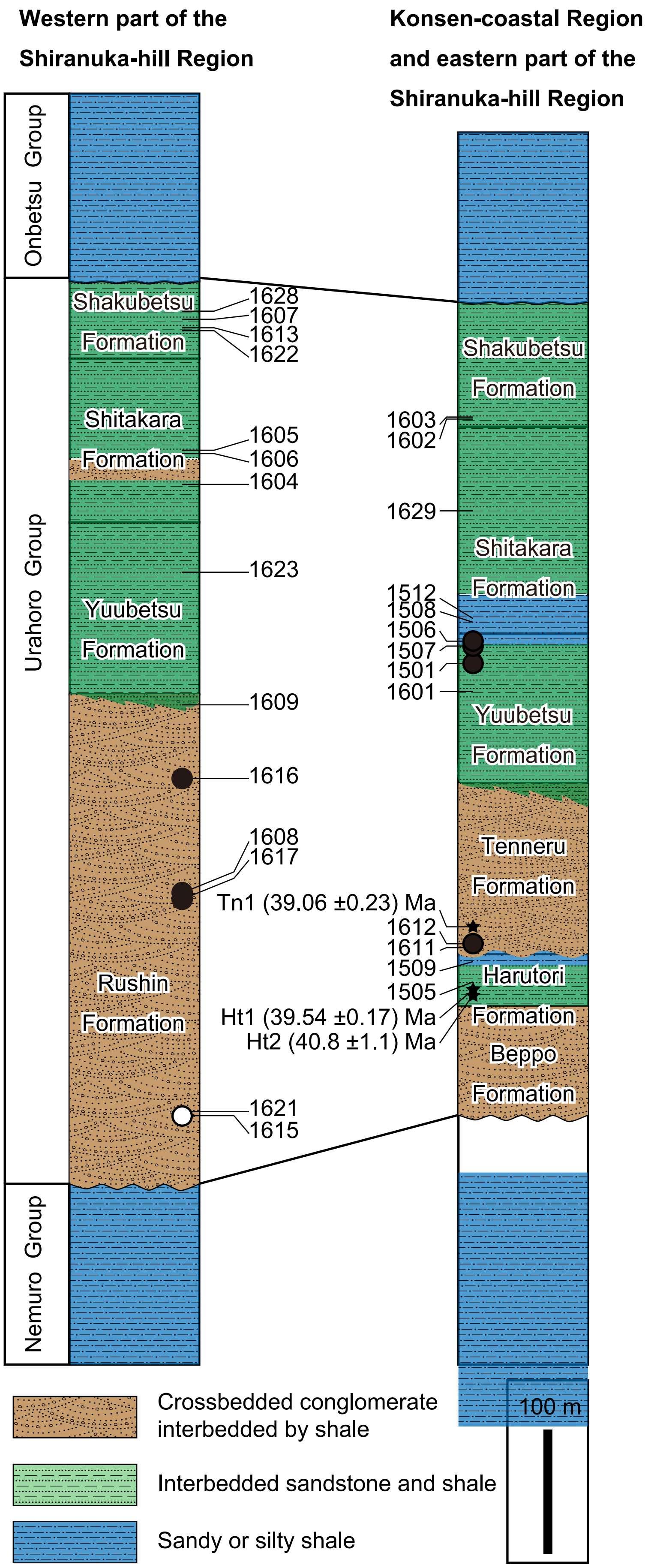

Figure 4. Stratigraphic relationships of horizons of the radiometric and paleomagnetic samples. Geological columns of the western region were made from a route map along the Satombetsu river section (Figure 3d). Columns of the eastern region were made from Miyasaka and Hoyanagi (2010). Black and white circles indicate normal and reversed paleomagnetic polarities, respectively.

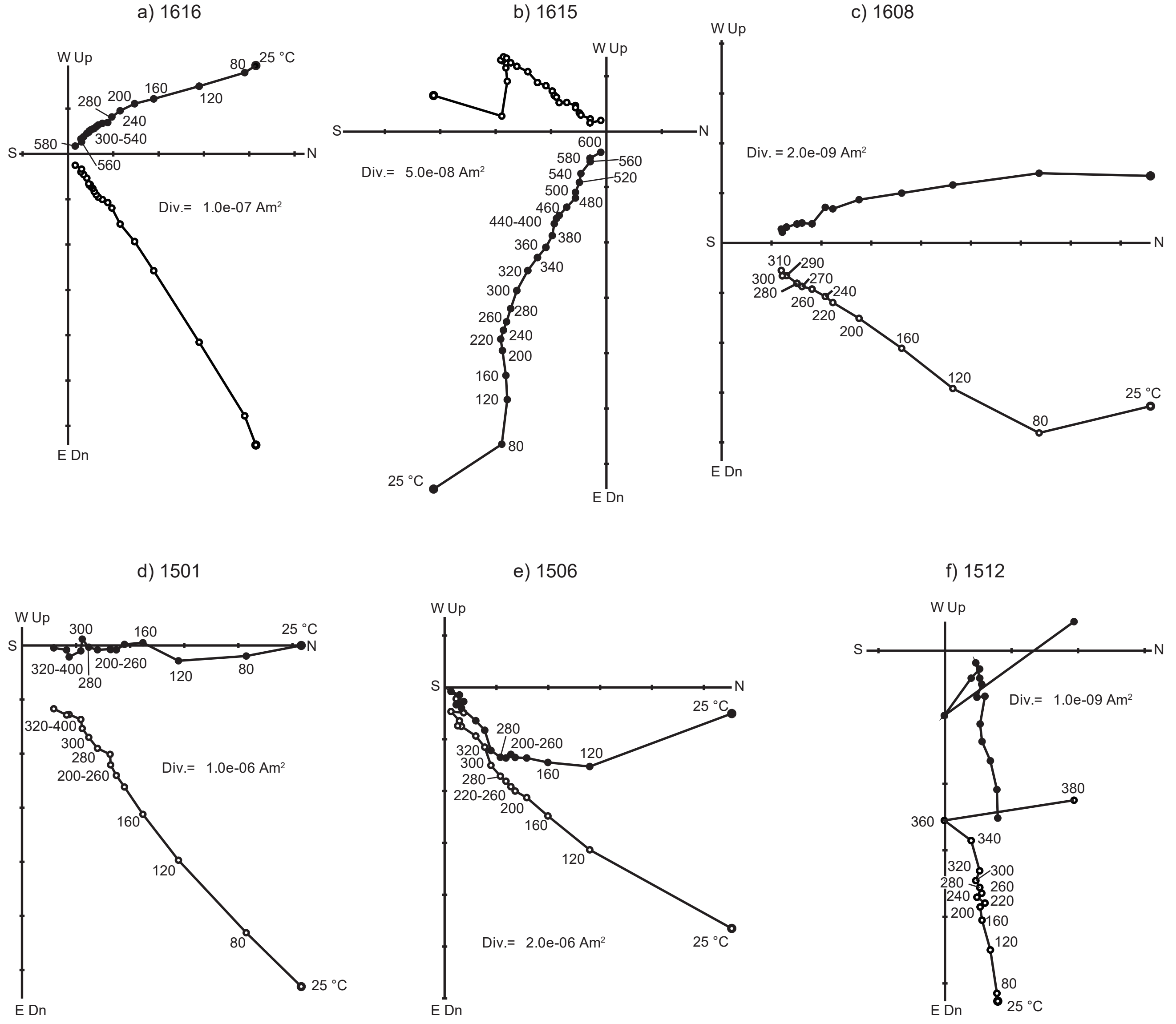

Figure 5. Examples of progressive demagnetization results displayed on orthogonal-endpoint diagrams. Polygonal lines with solid and open circles are on the horizontal and north-south vertical planes, respectively. Div., intensity of remanence for a division on axes of the orthogonal-endpoint diagrams (Am^2).

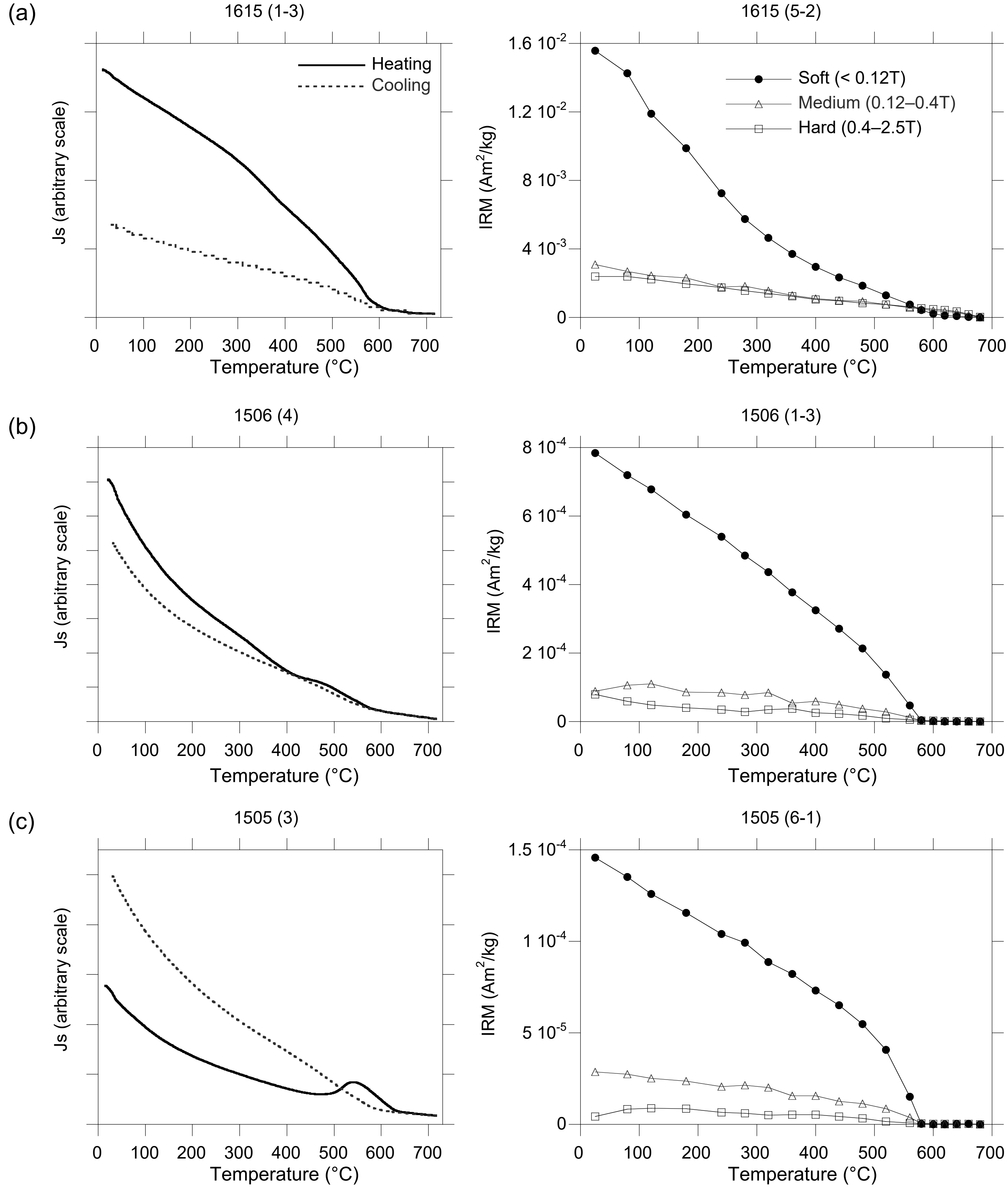

Figure 6. Typical results of strong-field thermomagnetic (left) and thermal demagnetization experiments of composite IRMs (right) for selected samples.

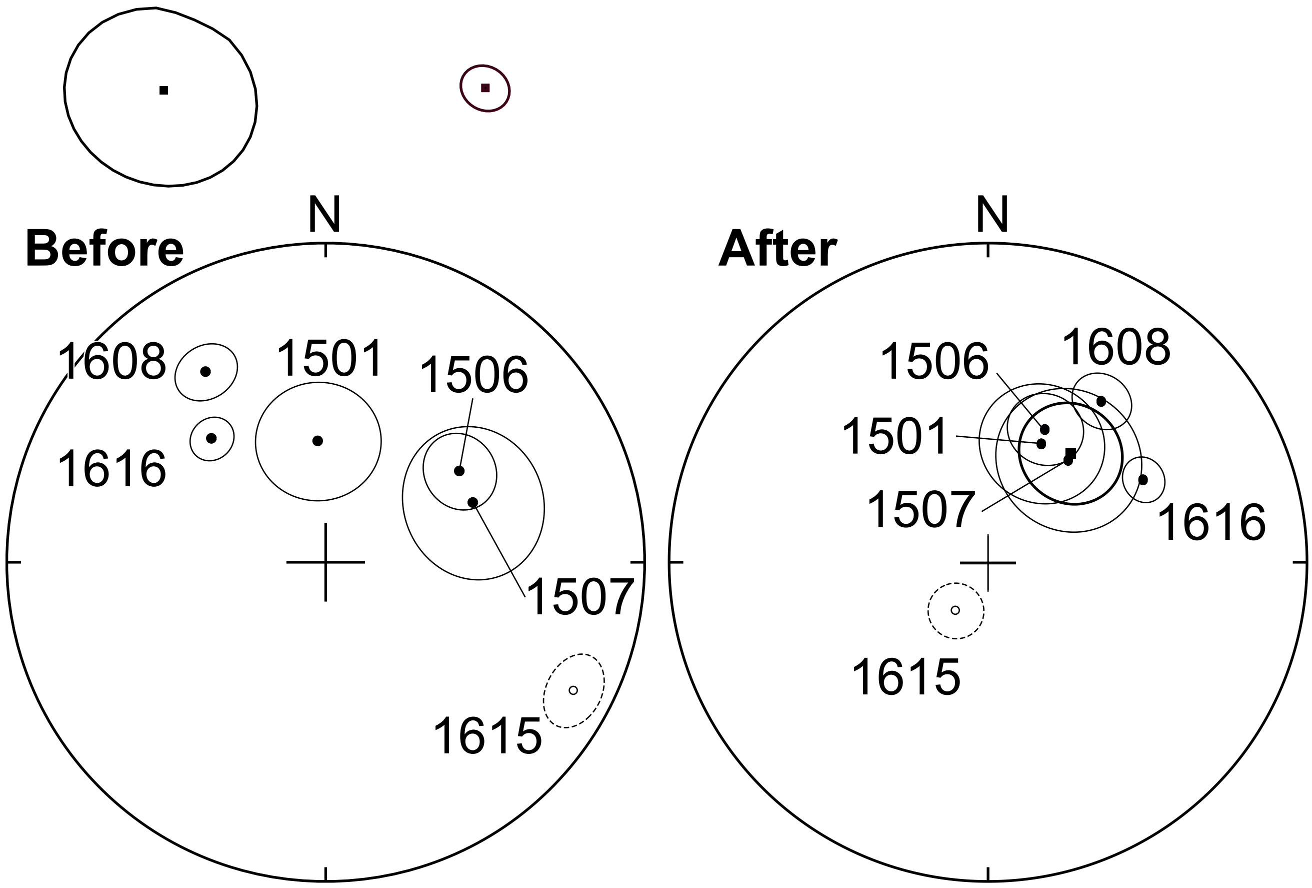

Figure 7. Equal-area plots of site mean directions from the Urahoro Group in the Shiranuka-hill region before and after tilt corrections. Solid and open symbols are on the lower and upper hemispheres, respectively. Ovals around the directions are 95% confidence limits. Numerals indicate site numbers.

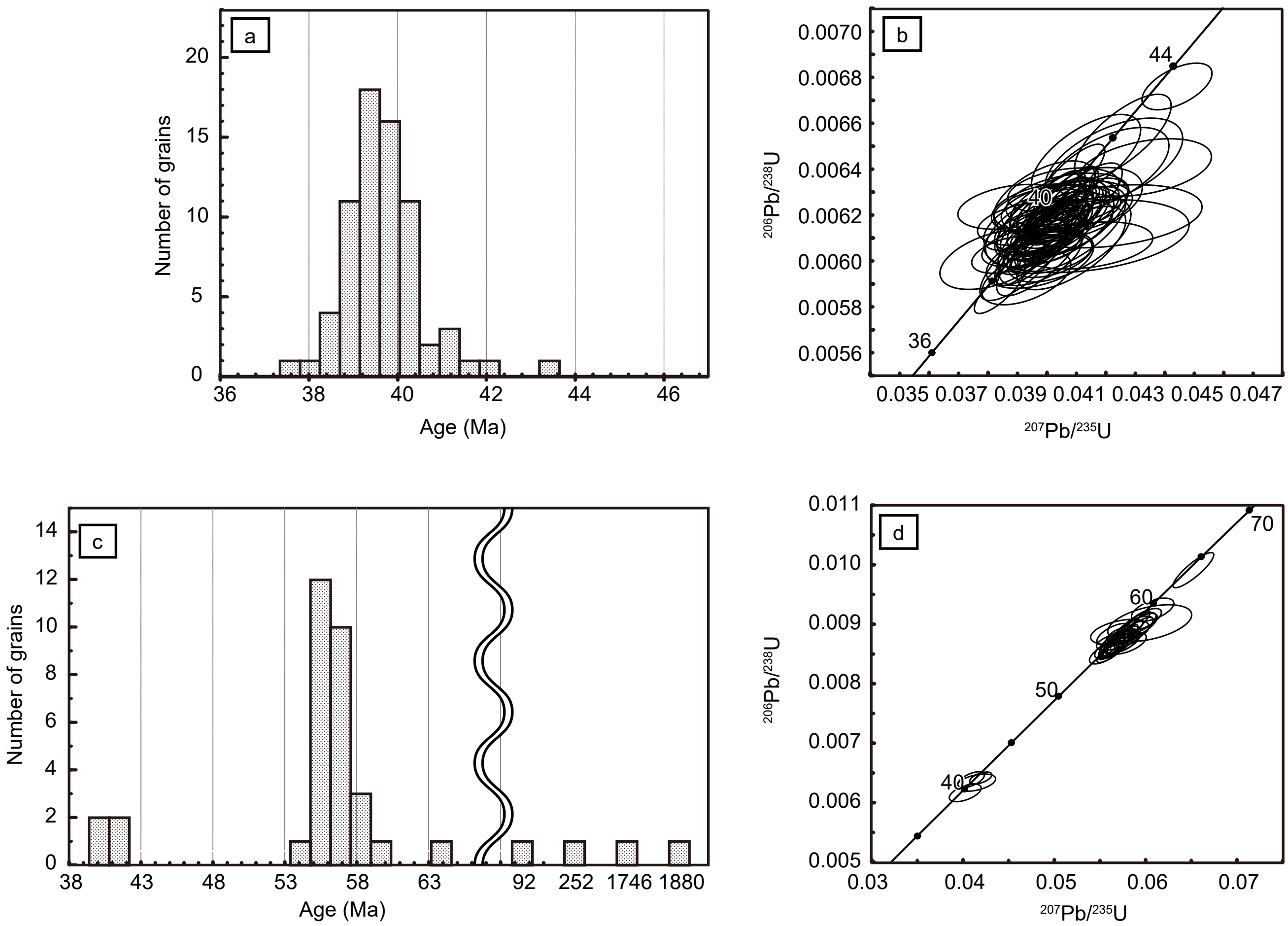

Figure 8. U-Pb ages for zircons in the tuffaceous layers in the Urahoro Group. (a) Histogram of all U-Pb radiometric age of individual grains obtained from Ht1, except for one exceptionally old age datum from grain S62. (b) Concordia plot of all concordant data except for the age obtained from grain S62. (c) Histogram of all concordant data obtained from Ht2. (d) Concordia plot of concordant data except for the clusters of 92 Ma, 252 Ma, 1746 Ma, and 1880 Ma.

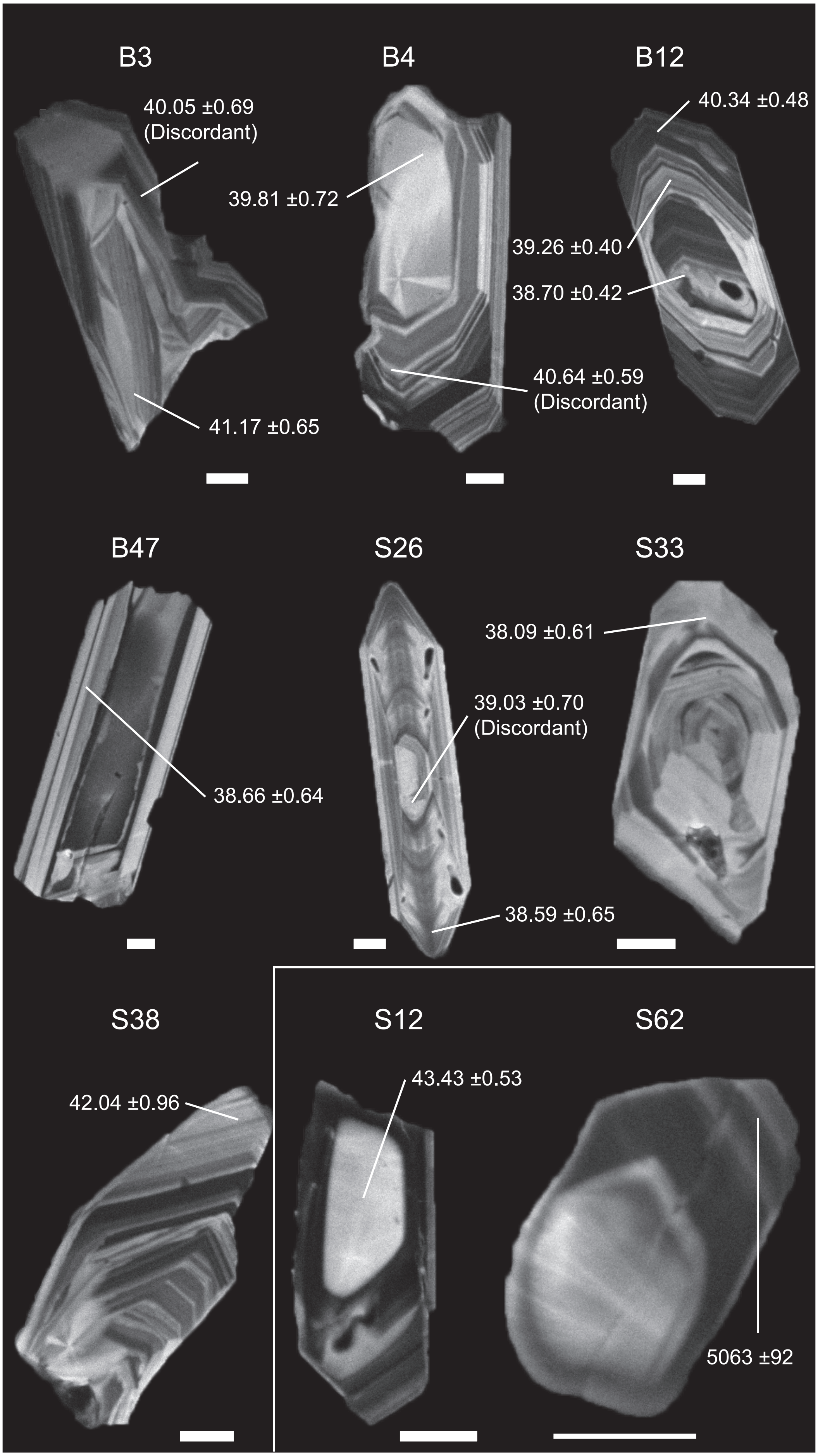

Figure 9. CL images of representative zircon grains from Ht1. Measured points are shown with their 206Pb/238U ages. Grains with relatively young, medium and old ages are shown by the upper, middle and lower lines, respectively. Scale bars are 20 μm long.

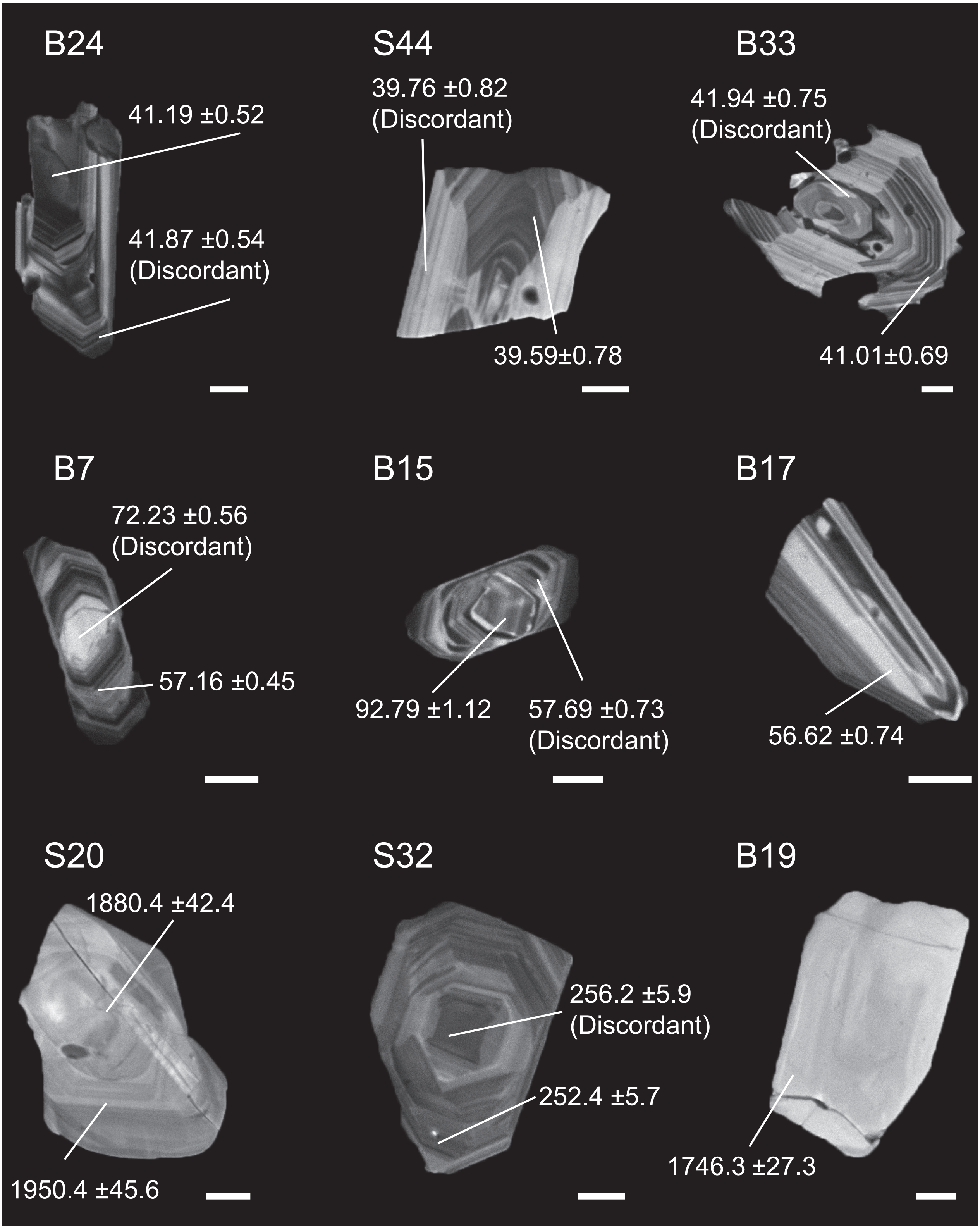

Figure 10. CL images of representative zircon grains obtained from Ht2. Measured points are shown with their $^{206}Pb/^{238}U$ ages. Scale bars are 20 μm long.

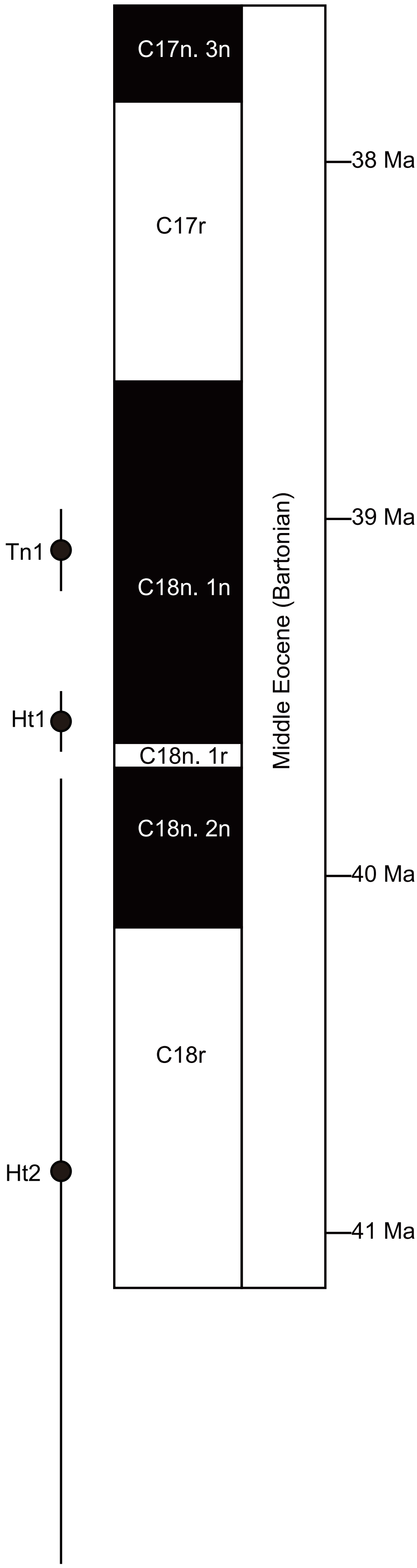

Figure 11. Correspondence of ages of tuffaceous beds with the geomagnetic polarity timescale of Ogg (2012).

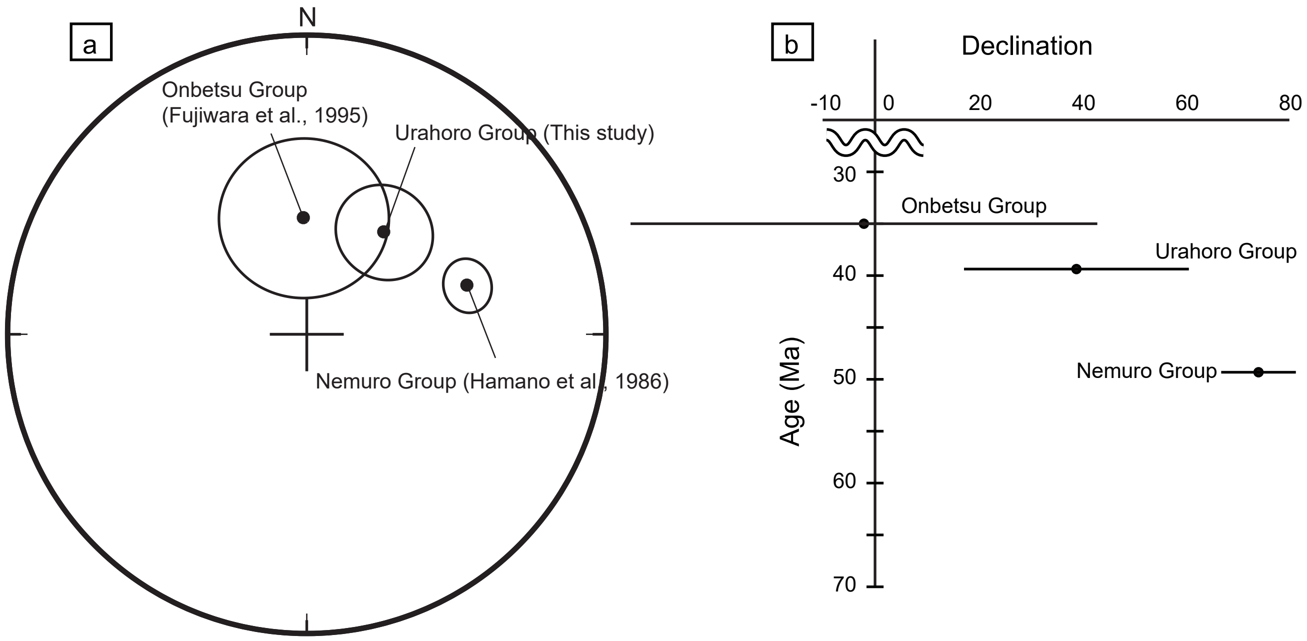

Figure 12. Paleomagnetic data in the Shiranuka-hill region. (a) Equal-area plots of paleomagnetic directions from the Nemuro, Urahoro and Onbetsu Groups (Fujiwara et al., 1995; Hamano et al., 1986). (b) Paleomagnetic declinations from the three groups, with 95% confidence limit, as a function of the depositional ages of the groups.

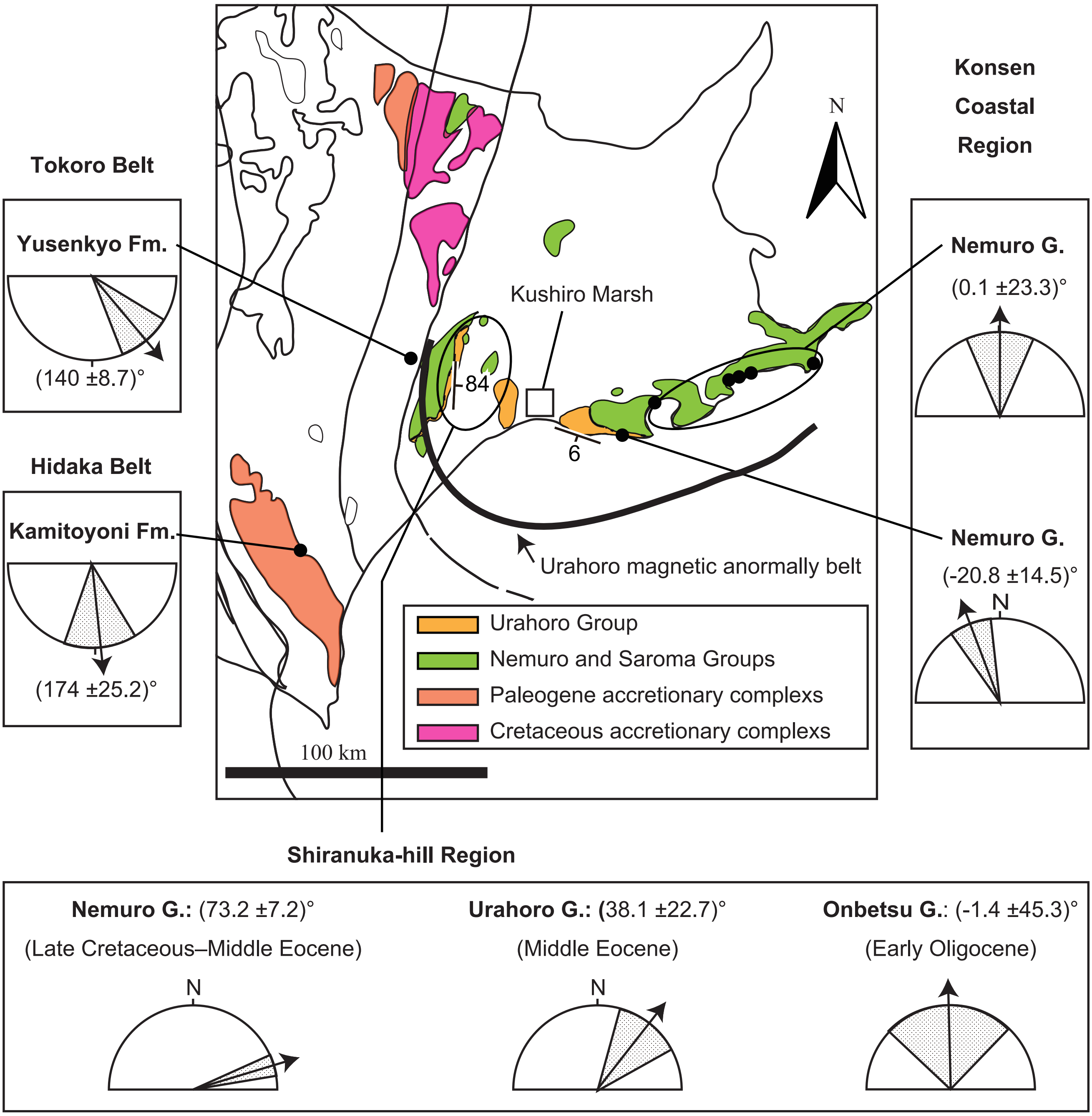

Figure 13. Distribution of terranes belonging to the Paleo-Kuril Arc (modified after Niida, 2010) and paleomagnetic declinations from the terrane with 95% confidence limits (Fujiwara et al., 1995; Fujiwara & Kanamatsu; 1990; Hamano et al., 1986; Nifuku et al., 2009). Yusenkyo Fm. was deposited in late Campanian–early Maastrichtian (Kanamatsu et al., 1992) and Kamitoyoni Fm. was deposited in the late Cretaceous to Paleocene (Nanayama, 1992). Fm., Formation. G., Group.

Table 1. Instrumentation and operational settings of the LA-ICP-MS technique for U-Pb dating.

Laser ablation system	Model	ESI NWR 193 (New Wave Research, Oregon, USA)
	Wavelength	193 nm
	Fluence	2.0 J/cm^2 (40%)
	Frequency	4 Hz
	Spot size	20 μm
	Pre Abration	1 shot (for cleaning)
	Carrier gas	He
	He gas flow	0.45 l/min
	Ar-make up gas flow	0.94 l/min
	Number of Shots	50 shots/spit
ICP-MS	Model	Nu Plasma Ⅱ MC-ICP-MS (Nu Instruments, Wrexham, UK)
	Analyzed isotopes	^{202}Hg, ^{204}(Pb+Hg), ^{206}Pb, ^{207}Pb, ^{208}Pb, ^{232}Th (Faraday), ^{238}U
	Integration time	12 s
Data analysis	Gas blank	Before, after and between individual mesurement
	Primary standard	Nancy 91500 (^{206}Pb / ^{238}U) NIST SRM610 (^{207}Pb / ^{206}Pb)
	Secondary standard	OD3

Table 2. Paleomagnetic data from the Urahoro Group.

Site	Lat	Long	Lithology	n_A/n	Levels	D_{IS}	I_{IS}	D_{TC}	I_{TC}	α95	κ	Polarity
1501	43.24	144.07	muddy sand	5/7	280–440	-3.5	55.9	24.5	53.3	16.7	18.7	N
1505	43.21	144.01	muddy sand	0/5	—	—	—	—	—	—	—	—
1506	43.23	144.00	muddy sand	6/8	280–480	56.0	44.3	23.4	49.2	10.0	45.5	N
1507	43.23	144.00	muddy sand	5/8	280–400	68.2	45.1	38.4	53.3	19.7	16.0	N
1508	43.23	144.00	muddy sand	0/5	—	—	—	—	—	—	—	—
1509	43.20	144.00	muddy sand	0/8	—	—	—	—	—	—	—	—
1512	43.24	144.07	muddy sand (nodule)	0/8	—	—	—	—	—	—	—	—
1601	43.23	144.07	muddy sand	0/6	—	—	—	—	—	—	—	—
1602	43.23	144.08	muddy sand	0/7	—	—	—	—	—	—	—	—
1603	43.23	144.08	muddy sand	0/8	—	—	—	—	—	—	—	—
1604	43.09	143.82	muddy sand	0/8	—	—	—	—	—	—	—	—
1605	43.09	143.82	muddy sand	0/7	—	—	—	—	—	—	—	—
1606	43.09	143.82	muddy sand	0/8	—	—	—	—	—	—	—	—
1607	43.09	143.83	muddy sand (nodule)	0/7	—	—	—	—	—	—	—	—
1608	43.09	143.82	muddy sand	6/8	280–320	-32.2	26.7	35.3	34.4	7.5	55.6	N
1609	43.09	143.82	muddy sand	0/7	—	—	—	—	—	—	—	—
1611	43.12	143.95	muddy sand	1/5	460–520	89.2	54.9	35.9	66.5	—	—	—
1612	43.12	143.95	muddy sand	4/8	280–320	35.9	40.2	23.9	1.3	31.4	9.5	N
1613	43.11	143.97	very-fine-grained sand	0/7	—	—	—	—	—	—	—	—
1615	43.09	143.82	muddy sand	8/8	280–600	117.4	-11.1	- 145.8	-73.9	7.8	50.9	R
1616	43.09	143.82	muddy sand	6/6	280–580	-42.7	42.7	62.1	40.3	5.8	134.0	N
1617	43.09	143.82	muddy sand	4/7	280–320	-24.0	34.2	43.8	32.1	40.9	10.2	N
1621	43.09	143.82	muddy sand	0/7	—	—	—	—	—	—	—	—
1622	43.11	143.97	very-fine-grained sand	0/8	—	—	—	—	—	—	—	—
1623	43.10	143.83	muddy sand	0/5	—	—	—	—	—	—	—	—
1627	43.09	143.83	muddy sand	0/7	—	—	—	—	—	—	—	—
1628	43.09	143.83	muddy sand (nodule)	0/7	—	—	—	—	—	—	—	—
1629	43.23	144.07	fine-grained	0/5	—	—	—	—	—	—	—	—
Overall mean		[6]		In situ		-12.0	49.5					
				Unfolded				37.3	51.5	13.9	24.3	

Footnotes: Lat, latitude (N°); Long, longitude (E°); n_A, number of specimens used in calculation of the site mean direction; n, number of samples collected from a site; D_{IS}, I_{IS}, in-situ declination and inclination, respectively; D_{TC}, I_{TC}, declination and inclination, respectively, after tilt correction and true north correction; N, normal polarity; R, reversed polarity; —, No data.

Table 3. Calculated $^{207}Pb/^{235}U$ and $^{206}Pb/^{238}U$ ages of zircon grains from Ht1.

Grain Nc	7/5Age	error	6/8Age	error
B1	48.85	1.59	39.32	0.59
B1 ○	40.07	0.80	39.36	0.52
B2	46.05	0.81	40.35	0.52
B3 ○	43.06	1.80	41.17	0.65
B3	44.71	2.26	40.05	0.69
B4 ○	41.89	2.51	39.81	0.72
B4	52.11	1.42	40.64	0.59
B5	155.30	3.04	45.82	0.67
B5 ○	40.23	0.93	39.84	0.54
B5	39.51	1.75	40.38	0.64
B6	39.62	0.89	38.80	0.52
B6	41.52	1.47	40.13	0.60
B6 ○	39.41	0.92	39.37	0.53
B8 ○	38.53	0.98	38.73	0.42
B8	39.58	0.68	38.56	0.37
B11 ○	40.37	1.50	40.53	0.51
B12	39.29	0.96	38.70	0.42
B12 ○	39.57	0.78	39.26	0.40
B12	41.62	1.34	40.34	0.48
B13 ○	39.01	1.10	38.94	0.44
B14	40.39	0.68	39.23	0.38
B16 ○	41.15	1.78	38.99	0.54
B17	42.74	2.36	39.60	0.62
B17	39.88	0.62	39.10	0.37
B18 ○	40.18	1.72	40.03	0.54
B19 ○	39.86	1.19	38.77	0.45
B19	37.68	2.12	39.03	0.64
B23	44.86	2.47	39.23	0.67
B24	41.20	0.68	39.37	0.45
B25 ○	40.19	0.93	39.66	0.49
B25	40.10	1.47	39.85	0.56
B25	41.77	1.08	38.71	0.49
B26 ○	39.67	1.37	40.04	0.55
B27 ○	40.00	0.95	39.96	0.49
B27	41.30	1.10	39.96	0.51
B28	41.69	1.13	39.02	0.50
B28 ○	39.63	1.26	39.21	0.53
B28	39.14	0.79	38.77	0.46
B30	782.42	10.98	102.40	1.66
B30 ○	39.44	1.07	38.99	0.92
B31 ○	40.55	1.68	39.16	0.97
B31	40.36	2.02	38.80	1.00
B32	74.20	2.33	42.02	1.03
B34	50.13	3.75	39.69	1.15
B34 ○	40.58	1.52	39.45	0.97
B35	41.83	1.20	41.19	0.98
B35 ○	39.87	1.05	39.38	0.92
B36 ○	40.63	1.47	38.92	0.95
B37	924.95	20.96	121.17	3.59

B37	○	39.61	1.19	38.71	0.92
B38	○	39.05	1.18	38.58	0.92
B39		42.53	2.14	39.09	1.01
B40		40.55	1.43	39.91	0.69
B40	○	40.02	0.99	39.50	0.64
B40		40.63	1.25	39.85	0.67
B41		39.29	1.01	39.82	0.65
B41	○	39.87	0.94	39.46	0.63
B42	○	41.13	2.77	39.25	0.83
B43		45.97	2.43	39.60	0.79
B44	○	40.24	1.13	39.72	0.66
B45	○	38.03	1.44	38.60	0.68
B46		40.17	1.26	39.82	0.67
B46	○	40.13	0.81	40.04	0.63
B47	○	39.61	1.12	38.66	0.64
B48		42.72	1.57	40.31	0.71
B49	○	38.65	1.45	40.07	0.51
B51	○	40.05	0.80	39.00	0.40
B51		39.58	2.13	38.70	0.59
B52	○	39.30	1.45	39.61	0.50
B52		36.74	1.76	38.58	0.54
B53		39.05	1.22	39.95	0.47
B53		40.12	0.63	39.30	0.38
S1		90.91	3.38	44.20	0.98
S1		41.52	0.90	40.04	0.74
S2		41.55	0.93	40.39	0.75
S3		70.03	1.86	46.59	0.91
S4	○	39.73	1.37	40.37	0.80
S5		45.35	2.26	39.40	0.87
S6		43.45	1.33	40.51	0.79
S7	○	39.85	0.85	39.45	0.73
S8		41.41	1.33	40.01	0.79
S9	○	40.78	1.80	40.14	0.84
S10		40.09	0.99	40.06	0.76
S10	○	40.61	0.92	40.89	0.76
S11	○	40.38	0.94	40.24	0.75
S12	○	44.12	0.94	43.43	0.53
S13	○	40.45	0.91	40.18	0.50
S14	○	39.32	0.78	38.93	0.47
S15	○	40.48	1.78	40.05	0.62
S16		46.41	1.46	39.11	0.55
S17		453.38	7.36	96.99	1.47
S17		42.99	1.11	40.07	0.52
S18	○	40.50	1.66	40.27	0.61
S19	○	39.99	1.11	38.72	0.51
S21	○	39.52	1.17	39.45	0.53
S22		41.06	1.07	39.62	0.51
S22	○	40.44	0.65	40.34	0.47
S23		47.17	1.12	42.18	0.54
S24		615.26	10.57	82.38	1.54
S25		171.74	2.54	46.84	0.69
S26		38.41	1.76	39.03	0.70
S26	○	39.59	1.46	38.59	0.65
S27	○	40.19	0.78	39.72	0.58

S28	○	38.25	0.69	37.77	0.55
S28		47.94	0.85	40.75	0.60
S29	○	40.12	0.80	40.32	0.60
S30	○	40.42	1.47	40.01	0.67
S31		42.51	0.97	41.35	0.63
S32	○	38.97	1.02	39.61	0.61
S33	○	39.14	1.21	38.09	0.61
S34	○	40.50	1.23	39.52	0.63
S35	○	39.49	1.14	38.96	0.88
S36		41.46	1.29	40.22	0.92
S37	○	42.04	1.86	41.33	1.00
S38	○	42.34	1.30	42.04	0.96
S39	○	40.11	1.02	39.46	0.88
S40		40.73	1.04	39.64	0.88
S41		42.50	1.01	39.63	0.88
S42		41.40	1.07	40.02	0.89
S43	○	39.98	1.47	39.74	0.93
S44	○	39.69	1.23	39.28	0.90
S45	○	40.36	1.08	39.54	0.89
S45	○	41.12	1.48	41.47	0.97
S46		40.77	0.99	39.82	0.88
S47		40.83	1.02	39.62	0.86
S48	○	40.16	1.06	39.59	0.86
S49		40.66	1.28	39.28	0.87
S50	○	41.80	1.68	41.12	0.95
S51	○	40.03	1.53	39.71	0.91
S52	○	40.75	1.43	39.77	0.90
S52		42.11	1.67	39.51	0.92
S53	○	39.74	1.01	40.02	0.87
S54	○	39.91	1.74	39.52	0.93
S54		48.67	1.75	40.81	0.94
S55	○	40.24	0.98	40.15	0.87
S56	○	40.88	1.17	40.22	0.88
S57		50.06	1.24	40.51	0.88
S58		41.61	1.19	39.06	0.71
S59		40.28	0.83	39.55	0.69
S60		40.79	0.86	39.99	0.70
S61		68.81	1.66	42.69	0.77
S62		5018.62	26.54	5063.27	91.84

Footnotes: 7/5 Age, $^{207}Pb/^{235}U$ age (Ma); 6/8 Age, $^{206}Pb/^{238}U$ age (Ma). Uncertainties are reported at the 2σ level. Data with circles in the left column were used in mean calculation of the mean.

Table 4. Calculated $^{207}Pb/^{235}U$ and $^{206}Pb/^{238}U$ ages of zircon grains from Ht2.

Grain No	7/5Age	error	6/8Age	error
B1	1803.77	39.05	613.09	23.76
B3	428.15	4.26	299.80	2.70
B4	198.69	1.84	157.49	1.24
B4	153.64	1.38	151.68	1.16
B5	55.49	0.82	54.89	0.46
B6	57.59	0.96	56.43	0.49
B7	130.81	1.23	72.23	0.56
B7	59.93	0.67	57.16	0.45
B8	56.49	0.68	56.23	0.44
B10	1503.94	6.55	446.30	3.36
B10	256.53	2.20	212.42	1.65
B11	78.56	1.02	58.14	0.48
B12	56.94	0.70	56.60	0.45
B12	56.49	1.26	56.29	0.71
B15	93.99	2.06	92.79	1.18
B15	65.10	1.44	57.69	0.73
B17	56.92	1.43	56.63	0.74
B18	55.77	1.42	55.83	0.74
B19	1750.98	21.33	1746.28	27.28
B20	59.89	1.33	58.36	0.74
B20	66.59	1.72	57.94	0.78
B21	71.85	1.52	57.02	0.71
B22	56.40	1.33	55.49	0.71
B23	61.47	1.45	57.36	0.74
B24 ○	41.74	0.97	41.19	0.52
B24	42.51	1.06	41.88	0.54
B25	59.93	1.81	59.29	1.03
B26	56.48	2.51	56.91	1.10
B27	58.52	1.45	57.85	0.96
B27	57.76	2.13	57.14	1.05
B31	59.08	1.45	58.26	0.96
B32	57.18	1.70	55.70	0.96
B33 ○	40.71	1.16	41.01	0.69
B33	43.77	1.53	41.94	0.75
B34	55.46	1.33	55.17	0.90
B38 ○	41.23	1.72	40.69	0.76
B39	60.05	1.42	55.76	0.91
B39	55.83	1.44	56.67	0.94
B40	56.49	1.68	55.80	0.96
S1	42.36	1.09	41.00	0.99
S3	64.19	1.74	63.55	1.54
S8	7662.74	180.90	18568.34	1084.02
S13	262.94	6.27	68.25	1.69
S14	169.28	4.29	158.91	3.87
S17	57.93	1.66	56.79	1.39
S20	1898.72	22.70	1880.42	42.37
S20	1931.99	23.96	1950.37	45.60
S21	59.62	3.60	57.86	1.61
S22	82.99	2.27	61.76	1.51

S23	57.78	1.53	57.49	1.39
S24	56.06	1.41	55.82	1.34
S25	56.55	1.50	56.03	1.35
S26	57.47	1.42	56.30	1.29
S27	56.00	1.45	55.50	1.27
S28	58.70	1.89	56.55	1.34
S28	58.31	1.80	56.62	1.33
S29	76.47	2.37	58.29	1.39
S30	57.21	1.41	56.53	1.29
S31	56.07	1.50	55.76	1.29
S32	257.86	6.01	256.23	5.86
S32	254.68	5.86	252.44	5.75
S33	55.89	1.49	55.19	1.27
S33	56.58	1.74	56.37	1.33
S34	56.41	1.54	55.64	1.29
S35	67.16	2.03	56.43	1.33
S35	67.89	1.79	59.29	1.11
S36	58.01	1.63	57.28	1.08
S39	59.41	1.69	57.65	1.09
S40	58.56	1.52	57.59	1.07
S43	73.58	1.69	57.25	1.05
S44 ○	40.09	1.40	39.59	0.78
S44	42.84	1.81	39.76	0.82
S45	63.85	1.77	53.27	1.01
S46	55.07	1.46	54.73	1.02

Footnotes: 7/5 Age, $^{207}Pb/^{235}U$ age (Ma); 6/8 Age, $^{206}Pb/^{238}U$ age (Ma). Uncertainties are reported at the 2σ level. Data with circles in the left column were used calculation of the mean.

Table 5. Paleomagnetic directions obtained from the Paleo-Kuril Arc.

Area / Rock Unit	Age	Location (°N)	Location (°E)	Directions D	I	α 95	κ	*n*	Δ D	Δ I	reference	Tectonic Parameters R	ΔR	F	ΔF	R.P
Shiranuka-hill region																
Onbetsu Group	Latest Eocene to Early Oligocene	43.1	143.8	-01.4	55.1	24.0	8.8	6	45.3	24.0	Fujiwara et al. (1995)	-8.6	45.5	4.3	24.1	East Asia: 30 Ma
Urahoro Group	Late Eocene	43.1	143.8	37.3	51.5	13.9	24.3	6	22.7	13.9	this study	28.0	23.3	6.8	14.4	East Asia: 40 Ma
Urahoro Group	Late Eocene	43.1	143.8	93.7	56.8	12.3	100.9	3	22.9	12.3	Fujiwara et al. (1995)	84.4	23.5	1.5	12.9	East Asia: 40 Ma
Nemuro Group	Late Cretaceous	43.1	143.8	73.2	39.5	7.2	—	—	9.3	7.2	Hamano et al. (1986)	61.9	12.3	21.3	8.8	East Asia: 50 Ma
Nemuro Group	Late Cretaceous			66.0	84.9	22.5	3.9	15	—	22.5	Fujiwara et al. (1995)					
Konsen-coastal region																
Nemuro Group	Late Cretaceous	43.0	144.6	-20.8	60.0	9.4	97.5	4	14.5	9.4	Nifuku et al. (2009)	-31.2	19.8	-0.2	10.1	East Asia: 60 Ma
	Late Cretaceous to Early Eocene	43.1	145.1	0.1	61.5	13.6	15.3	9	23.3	13.6	Fujiwara and Kanamatsu (1990)	-10.4	30.0	-1.5	14.1	East Asia: 60 Ma

Footnotes: D and I, tilt-corrected declination and inclination of the observed mean directions, respectively; ΔD and ΔI, 95% confidence limit of declination and inclination, respectively. ΔD = sin-1(sin(α95)/cos(I)), ΔI = α95; n, number of data points used in calculating mean directions; R and F, discrepancies in declination (R) and inclination (F) between the observed and expected directions; ΔR and ΔF, 95% confidence limits of R and F, respectively. Tectonic parameters were calculated based on the definition of Beck et al. (1980); —, no data; R. P., reference pole of East Asia from Cogné et al. (2013). Paleomagnetic directions and paleomagnetic pole positions of the previous studies, except for Hamano et al. (1986), were recalculated from site-mean directions with α95≦20. The positions of sampling sites in Fujiwara and Kanamatsu (1990) were assumed as follows: A, 43.05°N and 144.84°E; B, 43.14°N and 145.18°E; C, 43.15°N and 145.16°E; D, 43.19°N and 145.53°E; E43.15°N and 145.23°E.